

Video Super Resolution Based on Deep Learning: A Comprehensive Survey

Hongying Liu, *Member, IEEE*, Zhubo Ruan, Peng Zhao, Chao Dong, *Member, IEEE*,
Fanhua Shang, *Senior Member, IEEE*, Yuanyuan Liu, *Member, IEEE*, Linlin Yang

Abstract—In recent years, deep learning has made great progress in many fields such as image recognition, natural language processing, speech recognition and video super-resolution. In this survey, we comprehensively investigate 33 state-of-the-art video super-resolution (VSR) methods based on deep learning. It is well known that the leverage of information within video frames is important for video super-resolution. Thus we propose a taxonomy and classify the methods into six sub-categories according to the ways of utilizing inter-frame information. Moreover, the architectures and implementation details of all the methods are depicted in detail. Finally, we summarize and compare the performance of the representative VSR method on some benchmark datasets. We also discuss some challenges, which need to be further addressed by researchers in the community of VSR. To the best of our knowledge, this work is the first systematic review on VSR tasks, and it is expected to make a contribution to the development of recent studies in this area and potentially deepen our understanding to the VSR techniques based on deep learning.

Index Terms—Video super-resolution, deep learning, convolutional neural network, inter-frame Information.

I. INTRODUCTION

Super-resolution (SR) aims at recovering a high-resolution (HR) image or multiple images from the corresponding low-resolution (LR) counterparts. It is a classic and challenging problem in computer vision and image processing, and it has extensive real-world applications, such as medical image reconstruction [1], face [2], remote sensing [3] and panorama video super-resolution [4, 5], UAV surveillance [6] and high-definition television [7]. With the advent of the 5th generation mobile communication technology, larger size images or videos can be transformed within a shorter time. Meanwhile, with the popularity of high definition (HD) and ultra high definition (UHD) display devices, super-resolution is attracting more attention.

Video is one of the most common multimedia in our daily life, and thus super-resolution of low-resolution videos has become very important. In general, image super-resolution methods process a single image at a time, while video super-resolution algorithms deal with

multiple successive images/frames at a time so as to utilize relationship within frames to super-resolve the target frame. In a broad sense, video super-resolution (VSR) can be regarded as a class of image super-resolution and is able to be processed by image super-resolution algorithms frame by frame. However, the SR performance is always not satisfactory as artifacts and jams may be brought in, which causes unguaranteed temporal coherence within frames.

In recent years, many video super-resolution algorithms have been proposed. They mainly fall into two categories: the traditional methods and deep learning based methods. For some traditional methods, the motions are simply estimated by affine models as in [8]. In [9, 10], they adopt non-local mean and 3D steering kernel regression for video super-resolution, respectively. Liu and Sun [11] proposed a Bayesian approach to simultaneously estimate underlying motion, blur kernel, and noise level and reconstruct high-resolution frames. In [12], the expectation maximization (EM) method is adopted to estimate the blur kernel, and guide the reconstruction of high-resolution frames. However, these explicit models of high-resolution videos are still inadequate to fit various scenes in videos.

With the great success of deep learning in a variety of areas, super-resolution algorithms based on deep learning are studied extensively. Many video super-resolution methods based on deep neural networks such as convolutional neural network (CNN), generative adversarial network (GAN) and recurrent neural network (RNN) have been proposed. Generally, they employ a large number of both low-resolution and high-resolution video sequences to input the neural network for inter-frame alignment, feature extraction/fusion, and then to produce the high-resolution sequences for the corresponding low-resolution video sequences. The pipeline of most video super-resolution methods mainly includes one alignment module, one feature extraction and fusion module, and one reconstruction module, as shown in Fig. 1. Because of the nonlinear learning capability of deep neural networks, the deep learning based methods usually achieve good performance on many public benchmark datasets.

So far, there are few works about the overview on video super-resolution tasks, though many works [13, 14, 15] on the investigation of single image super-resolution have been published. Daithankar and Ruikar [16] pre-

H. Liu, Z. Ruan, P. Zhao, F. Shang, Y. Liu and L. Yang are with the Key Laboratory of Intelligent Perception and Image Understanding of Ministry of Education, School of Artificial Intelligence, Xidian University, China. E-mails: {hyliu, fhshang, yyliu}@xidian.edu.cn.

C. Dong is with the Shenzhen Institutes of Advanced Technology, Chinese Academy of Sciences. E-mail: chao.dong@siat.ac.cn.

Manuscript received November 12, 2020.

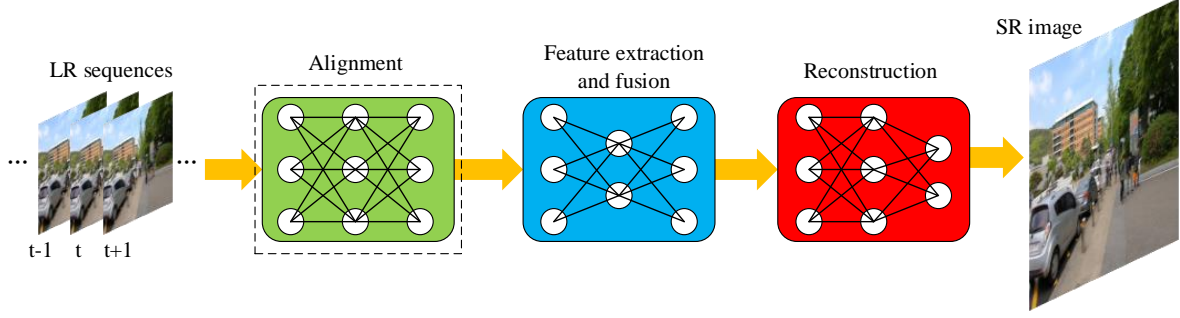


Fig. 1: The general pipeline of deep learning methods for VSR tasks. Note that the inter-frame alignment module can be either traditional methods or deep CNNs, while both the feature extraction & fusion module and the upsampling module usually utilize deep CNNs. The dashed line box means that the module is optional.

sented a brief review on many frequency-spatial domain methods, while the deep learning methods are rarely mentioned. Unlike the previous work, we provide a comprehensive investigation on deep learning techniques for video super-resolution in recent years. It is well known that the main difference between video super-resolution and image super-resolution lies in the processing of inter-frame information. How to effectively leverage the information from neighboring frames is critical for VSR tasks. We focus on the ways of utilizing inter-frame information for various deep learning based methods.

The contributions of this work are mainly summarized as follows. 1) We review recent works and progresses on developing techniques for deep learning based video super-resolution. To the best of our knowledge, this is the first comprehensive survey on deep learning based VSR methods. 2) We propose a taxonomy for deep learning based video super-resolution methods by categorizing their ways of utilization inter-frame information and illustrate how the taxonomy can be used to categorize existing methods. 3) We summarize the performance of state-of-the-art methods on some public benchmark datasets. 4) We further discuss some challenges and perspectives for video super-resolution tasks.

The rest of the paper is organized as follows. In Section II, we briefly introduce the background of video super-resolution. Section III shows our taxonomy for recent works. In Sections IV and V, we describe the video super-resolution methods with and without alignment, respectively, according to the taxonomy. In Section VI, the performance of state-of-the-art methods is analyzed quantitatively. In Section VII, we discuss the challenges and prospective trends in video super-resolution. Finally, we conclude this work in Section VIII.

II. BACKGROUND

Video super-resolution stems from image super-resolution, and it aims at restoring high-resolution videos from multiple low-resolution frames. However, the difference between video and image super-resolution techniques is also obvious, that is, the former usually takes advantage of inter-frame information. Besides the

RGB color space, the YUV including YCbCr color space is also widely used for VSR. $I_i \in \mathbb{R}^{H \times W \times 3}$ denotes the i -th frame in a LR video sequence I , and $\hat{I}_i \in \mathbb{R}^{sH \times sW \times 3}$ is the corresponding HR frame, where s is the scale factor, e.g., $s = 2, 4$, or 8 . And $\{\hat{I}_j\}_{j=i-N}^{i+N}$ is a set of $2N+1$ HR frames for the center frame \hat{I}_i , where N is the temporal radius. Then the degradation process of HR video sequences can be formulated as follows:

$$I_i = \phi(\hat{I}_i, \{\hat{I}_j\}_{j=i-N}^{i+N}; \theta_\alpha) \quad (1)$$

where $\phi(\cdot; \cdot)$ is the degradation function, and the parameter θ_α represents various degradation factors such as noise, motion blur and downsampling factors. In most existing works such as [11, 12, 17, 18], the degradation process is expressed as:

$$I_j = DBE_{i \rightarrow j} \hat{I}_i + n_j \quad (2)$$

where D and B are the down-sampling and blur operations, n_j denotes image noise, and $E_{i \rightarrow j}$ is the warping operation based on the motion from \hat{I}_i to \hat{I}_j .

In practice, it is easy to obtain LR image I_j , but the degradation factors, which may be quite complex or probably a combination of several factors, are unknown. Different from single image super-resolution (SISR) aiming at solving a single degraded image, VSR needs to deal with degraded video sequences, and recovers the corresponding HR video sequences, which should be as close as the ground truth (GT) videos. Specifically, a VSR algorithm may use similar techniques to SISR for processing a single frame (spatial information), while it has to take relationships among frames (temporal information) into consideration to ensure motion consistency of the video. The super-resolution process, namely the reverse process of Eq. (1), can be formulated as follows:

$$\tilde{I}_i = \phi^{-1}(I_i, \{I_j\}_{j=i-N}^{i+N}; \theta_\beta) \quad (3)$$

where \tilde{I}_i denotes the estimation of the GT (i.e., \hat{I}_i), and θ_β is the model parameter.

Like SISR, video quality is mainly evaluated by calculating peak signal-noise ratio (PSNR) and structural

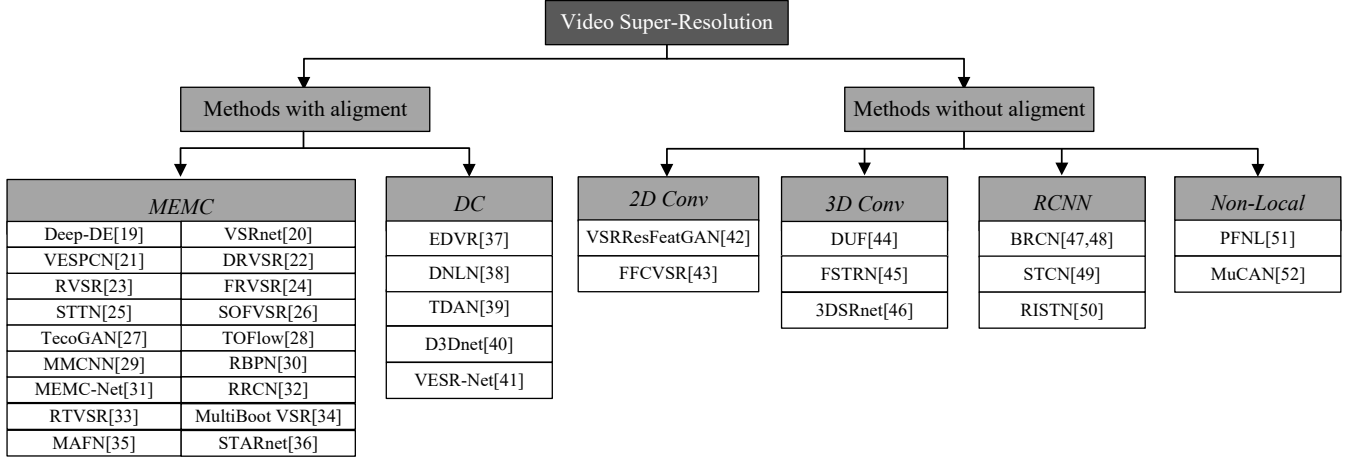


Fig. 2: A taxonomy for existing state-of-the-art video super-resolution methods. Here, *MEMC* stands for motion estimation and compensation methods, *DC* is deformable convolution methods, *3D Conv* is 3D convolution methods, and *RCNN* denotes recurrent convolutional neural network based methods.

similarity index (SSIM). These indexes measure the difference of pixels and similarity of structures between two images, respectively.

III. VIDEO SUPER-RESOLUTION METHODS

As the videos are a recording of moving visual images and sound, the methods for video super-resolution learn from existing single image super-resolution methods. There are many deep learning based image super-resolution methods such as SRCNN [53], FSRCNN [54], VDSR [55], ESPCN [56], RDN [57], RCAN [58], ZSSR [59] and SRGAN [60]. In 2016, based on SRCNN, Kappeler [20] presented a video super-resolution method with convolutional neural networks (VSRnet). So far, many video super-resolution algorithms have been proposed. In the following, we summarize the characteristics of the deep learning based methods for video super-resolution in recent years, as shown in Table I.

Several studies such as [37, 44, 39] on video super-resolution have indicated that the utilization of information between frames greatly influences performance. The proper and adequate usage of such information can enhance the results of super-resolution. Therefore, we build a taxonomy for existing video super-resolution methods according to their ways of the utilization of inter-frame information, as shown in Fig. 2.

As shown in Fig. 2 and Table I, we categorize the existing methods into two main categories: methods with alignment and methods without alignment, according to whether the video frames are explicitly aligned. We will present the methods in detail in the following sections.

IV. METHODS WITH ALIGNMENT

The methods with alignment make neighboring frames explicitly align with the target frame by using extracted motion information before subsequent reconstruction. And the methods mainly use motion estimation and motion compensation (MEMC) or deformable

convolution, which are two common techniques for aligning frames. Next we will introduce state-of-the-art methods based on each of the techniques in detail.

A. Motion Estimation and Compensation Methods

In the methods with alignment for video super-resolution, most of them apply the motion estimation and motion compensation techniques. Specifically, the purpose of motion estimation is to extract inter-frame motion information, while motion compensation is used to perform the warping operation between frames according to inter-frame motion information and to make one frame align with another frame. A majority of the motion estimation techniques are performed by the optical flow method [61]. This method tries to calculate the motion between two neighboring frames through their correlations and variations in the temporal domain. The motion compensation methods can be divided into two categories: traditional methods (e.g., LucasKanade [62] and Druleas [63]) and deep learning methods such as FlowNet [61], FlowNet 2.0 [64] and SpyNet [65].

In general, an optical flow method takes two frames (e.g., I_i and I_j) as inputs. One is the target frame and the other is the neighboring frame. Then the method computes a vector field of optical flow $F_{i \rightarrow j}$ from the frame I_i to I_j by the following formula:

$$F_{i \rightarrow j}(h_{i \rightarrow j}, v_{i \rightarrow j}) = ME(I_i, I_j; \theta_{ME}) \quad (4)$$

where $h_{i \rightarrow j}$ and $v_{i \rightarrow j}$ is the horizontal and vertical components of $F_{i \rightarrow j}$, $ME(\cdot)$ is a function used to compute optical flow, and θ_{ME} is its parameter.

The motion compensation is used to perform image transformation between images in terms of motion information to make neighboring frames align with the target frame. It can be achieved by some methods such as bilinear interpolation and spatial transformer network (STN) [66]. In general, a compensated frame I'_j is expressed as:

$$I'_j = MC(I_i, F_{i \rightarrow j}; \theta_{MC}) \quad (5)$$

TABLE I: Existing video super-resolution methods based on deep learning and their key strategies. Here, *MEMC* is motion estimation and motion compensation, *DC* is deformable convolution, *3D Conv* is 3D convolution, and *RCNN* denotes recurrent convolutional neural networks.

Method	Year	Synonym	Type	Loss function	Align
Deep-DE [19]	2015	Deep Draft-Ensemble Learning	MEMC	ℓ_1 -norm loss with total variation regularization	✓
VSRnet [20]	2016	Video Super-Resolution with convolutional neural Networks		Mean Square Error (MSE) loss	✓
VESPCN [21]	2017	Video Efficient Sub-pixel Convolutional Network		MSE loss and Motion Compensation (MC) loss	✓
DRVSR [22]	2017	Detail-Revealing deep Video Super-Resolution		MSE loss and MC loss	✓
RVSR [23]	2017	Robust Video Super-Resolution		Spatial alignment loss and spatio-temporal adaptive loss	✓
FRVSR [24]	2018	Frame-Recurrent Video Super-Resolution		MSE loss and MC loss	✓
STTN [25]	2018	Spatio-Temporal Transformer Network		MSE loss and MC loss	✓
SOFVSR [26]	2018	Super-resolution Optical Flow for Video Super-Resolution		MSE loss and MC loss	✓
TecoGAN [27]	2018	Temporally coherent GAN		MSE loss and ping-pong loss etc.	✓
TOFlow [28]	2019	video enhancement with Task-Oriented Flow		ℓ_1 -norm loss	✓
MMCNN [29]	2019	Multi-Memory Convolutional Neural Network		MSE loss and MC loss	✓
RBPNet [30]	2019	Recurrent Back-Projection Network		ℓ_1 -norm loss	✓
MEMC-Net [31]	2019	Motion Estimation and Motion Compensation Network		Charbonnier (Cb) loss	✓
RRCN [32]	2019	Residual Recurrent Convolutional Network		MSE loss	✓
RTVSR [33]	2019	Real-Time Video Super-Resolution		MSE loss	✓
MultiBoot VSR[34]	2019	Multi-stage multi-reference Bootstrapping for Video Super-Resolution		Huber loss	✓
MAFN [35]	2020	Motion-Adaptive Feedback Network		MSE loss	✓
STARnet [36]	2020	Space-Time-Aware multi-Resolution network		Three losses	✓
EDVR [37]	2019	Enhanced Deformable convolutional networks for Video Restoration	DC	Cb loss	✓
DNLN [38]	2019	Deformable Non-Local Network for Video Super-Resolution		ℓ_1 -norm loss	✓
TDAN [39]	2020	Temporally-Deformable Alignment Network for Video Super-Resolution		ℓ_1 -norm loss	✓
D3Dnet [40]	2020	Deformable 3D Convolution for Video Super-Resolution		MSE loss	✓
VESR-Net [41]	2020	Video Enhancement and Super-Resolution Network		ℓ_1 -norm loss	✓
VSRResFeatGAN [42]	2019	Video Super-Resolution with Residual Networks	2D Conv	Adversarial loss; content loss; and perceptual loss	×
FFCVSR [43]	2019	Frame and Feature-Context Video Super-Resolution		MSE loss	×
DUF [44]	2018	video super-resolution network using Dynamic Upsampling Filters	3D Conv	Huber loss	×
FSTRN [45]	2019	Fast Spatio-Temporal Residual Network for Video Super-Resolution		Cb loss	×
3DSRnet [46]	2019	3D Super-Resolution Network		MSE loss	×
BRCN [47, 48]	2015/2018	video super-resolution via Bidirectional Recurrent Convolutional Networks	RCNN	MSE loss	×
STCN [49]	2017	Spatio-Temporal Convolutional Network for Video Super-Resolution		MSE loss	×
RISTN [50]	2019	Residual Invertible Spatio-Temporal Network for Video Super-Resolution		MSE loss	×
PFNL [51]	2019	Progressive Fusion network via exploiting Non-Local spatio-temporal correlations	Non-Local	Cb loss	×
MuCAN [52]	2020	Multi-Correspondence Aggregation Network for Video Super-Resolution		Edge-aware loss	×

where $MC(\cdot)$ is a motion compensation function, I_i , $F_{i \rightarrow j}$ and θ_{MC} are the neighboring frame, optical flow and the parameter. An example of motion estimation and motion compensation is shown in Fig. 3. Below we depict some representative methods in this category.

1) *Deep-DE*: The deep draft-ensemble learning method (Deep-DE)¹ [19] has two phases, as shown in Fig. 4. It first generates a series of SR drafts by adjusting the TV- ℓ_1 flow [67, 68] and the motion detail preserving (MDP) [69]. Then both the SR drafts and the bicubic-interpolated LR target frame are fed into a CNN for feature extraction, fusion and super-resolution.

The CNN in Deep-DE consists of four convolutional layers: the first three layers are general convolutional layers, and the last layer is a deconvolution layer. Their

kernel sizes are 11×11 , 1×1 , 3×3 and 25×25 , respectively, and the numbers of channels are 256, 512, 1 and 1.

2) *VSRnet*: VSRnet² [20] is based on the image super-resolution method, SRCNN [53], and its network architecture is shown in Fig. 5. VSRnet mainly consists of motion estimation and compensation modules, and three convolutional layers, and each convolutional layer is followed by a rectified linear unit (ReLU) except for the last one. The main difference between VSRnet and SRCNN is the number of input frames. That is, SRCNN takes a single frame as input, while VSRnet uses multiple successive frames, which are compensated frames. The motion information between frames is computed by the Druleas algorithm [63]. In addition, VSRnet proposes a filter symmetry enforcement (FSE) mechanism and an

¹Code: <http://www.cse.cuhk.edu.hk/leojia/projects/DeepSR/>

²Code: <https://superresolution.tf.fau.de/>

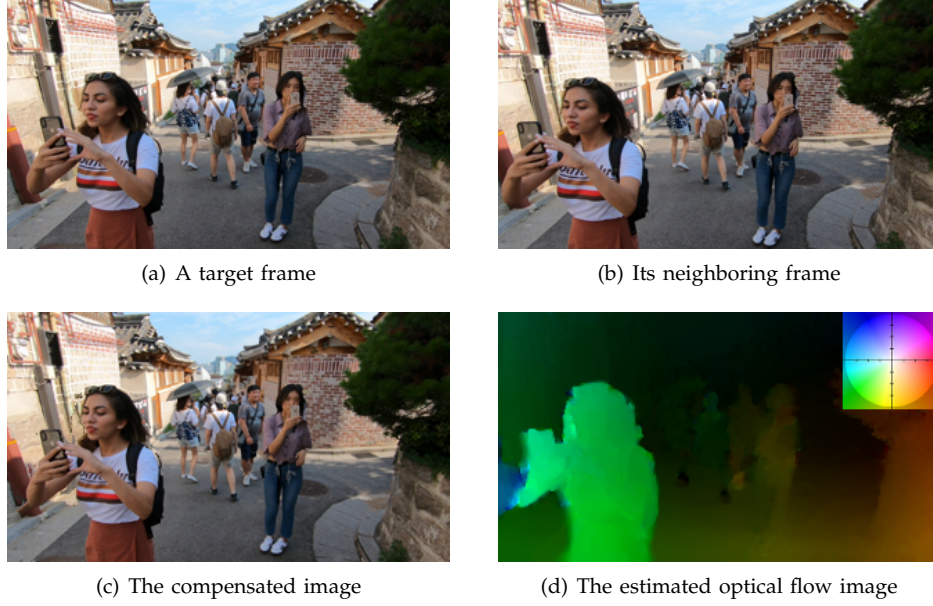


Fig. 3: An example of motion estimation and compensation. Note that the small rightmost image is the legend of (d). Different colors represent different directions of motion and the intensity of the color is the range of motion.

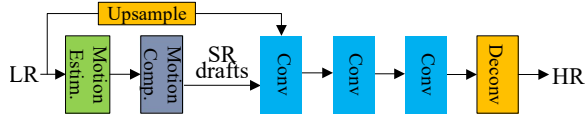


Fig. 4: The architecture of Deep-DE [19]. Here Motion Estim. is a motion estimation block, Motion Comp. is a motion compensation block, Conv is a convolutional layer and Deconv is a deconvolutional layer.

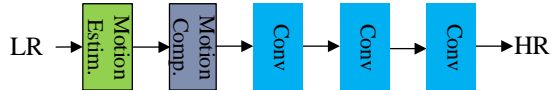


Fig. 5: The network architecture of VSRnet [20].

adaptive motion compensation mechanism, which are separately used to accelerate training and reduce the impact of unreliable compensated frames, and thus can improve video super-resolution performance.

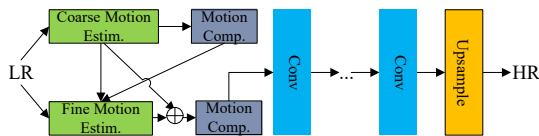


Fig. 6: The network architecture of VESPCN [21]. Here \oplus denotes element-wise sum.

3) *VESPCN*: The video efficient sub-pixel convolutional network (VESPCN) [21] proposes a spatial motion compensation transformer (MCT) module for motion estimation and compensation. Then the compensated frames are fed into a series of convolutional layers for feature extraction and fusion, as shown in Fig. 6. Finally,

the super-resolution results are obtained through a sub-pixel convolutional layer for upsampling.

The MCT module adopts CNNs to extract motion information and perform motion compensation. MCT uses a coarse-to-fine approach to compute the optical flow for image sequences. Firstly, in the coarse estimation stage, the network takes two consecutive frames (i.e., the target frame and a neighboring frame) as inputs. The coarse network consists of 5 convolutional layers and a sub-pixel convolutional layer. And it first performs the $\times 2$ downsampling operation two times and then performs the $\times 4$ upsampling operation by a sub-pixel convolutional layer to get coarse optical flow estimation results. Secondly, the neighboring frame is warped according to the optical flow. In the fine estimation stage, the target frame, neighboring frame, optical flow computed in the coarse stage and the warped neighboring frame are the input of the fine network, whose architecture is similar to the coarse network. It first conducts $\times 2$ downsampling and then perform $\times 2$ upsampling at the end of the network to attain the fine optical flow. Together with the coarse optical flow, the fine optical flow is used to obtain the final estimation result. Finally, the neighboring frame is warped again by the final optical flow to make the warped frame align with the target frame.

4) *DRVSR*: The detail-revealing deep video super-resolution (DRVSR)³ [22] method proposes a sub-pixel motion compensation layer (SPMC) that can perform the up-sampling and motion compensation operations simultaneously for neighboring input frames according to the estimated optical flow information. The network architecture of DRVSR is illustrated in Fig. 7.

³Code: https://github.com/jiangsutx/SPMC_VideoSR

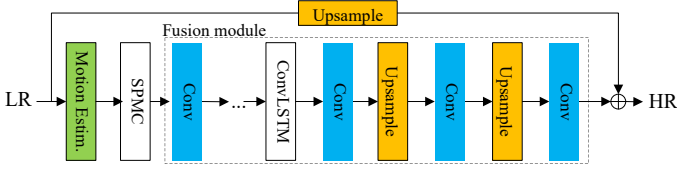


Fig. 7: The network architecture of DRVSR [22]. Here SPMC denotes a sub-pixel motion compensation layer, ConvLSTM is the convolutional LSTM [70].

DRVSR consists of three main modules: a motion estimation module, a motion compensation module using the SPMC layer, and a fusion module. The motion estimation module is implemented by the motion compensation transformer (MCT) network [21]. The SPMC layer consists of two sub-modules, namely grid generator and sampler. The grid generator first transforms the coordinates in the LR space into the coordinates in the HR space according to the optical flow, and then the sampler performs the interpolation operation in the HR space. In the fusion module, it applies the convolution with stride 2 to perform down-sampling and then conducts the deconvolution for up-sampling to obtain the HR residual image of the target frame. Together with the upscaled LR target frame, this residual image yields the final result. DRVSR also adopts the ConvLSTM module [70] to handle spatio-temporal information.

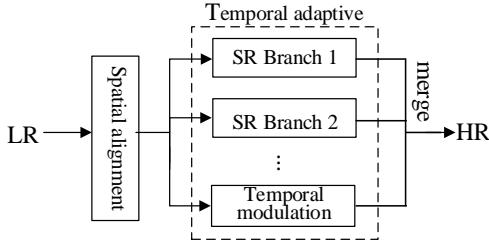


Fig. 8: The network architecture of RVSR [23], where SR denotes Super-Resolution.

5) *RVSR*: Robust video super-resolution (RVSR) [23] proposes a spatial alignment module to attain great alignment performance and a temporal adaptive module to adaptively determine the optimal scale of temporal dependency. And its architecture is shown in Fig. 8.

The spatial alignment module is responsible for the alignment of the multi-frames so that the neighboring frames are aligned with the target frame. It first estimates the transformation parameters between the neighboring frame and the target frame through a localization net, and then makes the neighboring frame align with the target frame through a spatial transformation layer [66] based on the obtained parameters. The localization net consists of two convolutional layers, each of which is followed by a max-pooling layer, and two fully connected layers. The temporal adaptive module is composed of multiple branches of SR subnetwork and a temporal modulation. Each subnetwork is responsible for han-

dling a temporal scale (i.e., the number of input frames), and outputting the corresponding super-resolution result. Then the super-resolution result of each subnetwork is allocated a weight through the temporal modulation. The final super-resolution result is the weight sum of the super-resolution result of each branch and its weight. The number of the input frames of the temporal modulation module is identical to the maximum number of input frames in the super-resolution network, and the network structure of the temporal modulation module is the same as that of the super-resolution network, and both of them are based on the structure of ESPCN [56].

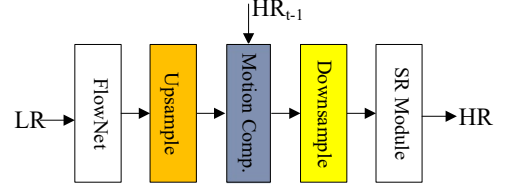


Fig. 9: The network architecture of FRVSR [24]. Here FlowNet is an optical flow estimation module, and SR Module is a super-resolution module.

6) *FRVSR*: Frame recurrent video super-resolution (FRVSR)⁴ [24] mainly proposes to use the previously inferred HR estimate to super-resolve the subsequent frame for producing temporally consistent results and reducing computational cost. The architecture of FRVSR is illustrated in Fig. 9.

The detailed implementation adopts an optical estimation network to compute the optical flow from the previous frame to the target frame. Then the LR optical flow is upsampled to the same size with the HR video by bilinear interpolation. The HR variant of the previous frame is warped by the upsampled LR optical flow, and then the warped HR frame is downsampled by space-to-depth transformation to get the LR version. Finally, the LR variant of the warped HR frame and the target frame are fed into the subsequent super-resolution network to attain the result for the target frame. In FRVSR, the optical flow network consists of 14 convolutional layers, 3 pooling layers and 3 bilinear upsampling layers. Each convolutional layer is followed by a LeakyReLU activation function, except for the last convolutional layer. The super-resolution network consists of 2 convolutional layers, 2 deconvolution layers with $\times 2$ and 10 residual blocks, where each residual block consists of 2 convolutional layers and a ReLU activation function.

7) *STTN*: Spatio-temporal transformer network (STTN) [25] proposes a spatio-temporal transformer module, which is used to address the problem that previous optical flow methods only process a pair of video frames, which may cause inaccurate estimation when occlusion and luminance variation exist in videos. The proposed module can handle multiple frames at a time. The architecture of STTN is illustrated in Fig. 10.

⁴Code: <https://github.com/msmsajjadi/FRVSR>

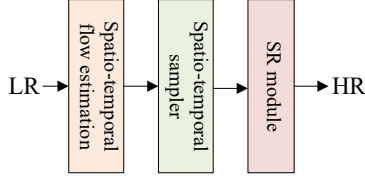


Fig. 10: The network architecture of STTN [25].

STTN consists of three major modules: a spatio-temporal flow estimation module, a spatio-temporal sampler module, and a super-resolution module. The spatio-temporal flow estimation module is a U-style network, similar to U-Net [71], consisting of 12 convolutional layers and two up-sampling layers. It first performs $\times 4$ downsampling, and then $\times 4$ up-sampling to restore the size of the input frames. This module is responsible for optical flow estimation of the consecutive input frames including the target frame and multiple neighboring frames, and the final output is a 3-channel spatio-temporal flow that expresses the spatial and temporal changes between frames. The spatio-temporal sampler module is actually a trilinear interpolation method, which is responsible for performing warp operation for current multiple neighboring frames and obtaining the aligned video frames according to the spatio-temporal flow obtained by the spatio-temporal flow module. For video super-resolution, the aligned frames can then be fed into the super-resolution (SR) module for feature fusion and super-resolution of the target frame.

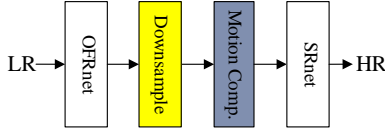


Fig. 11: The network architecture of SOFVSR [26]. Here, OFRnet is an optical flow network, and SRnet is a super-resolution module.

8) *SOFVSR*: Super-resolution optical flow for video super-resolution (SOFVSR)⁵ [26] is proposed to super-resolve LR estimated optical flow for attaining great SR performance. And its architecture is shown in Fig. 11.

The optical flow between frames is estimated by a coarse-to-fine approach including the optical flow reconstruction network (OFRnet), which finally yields a high-resolution optical flow. Then the HR optical flow is converted to the LR optical flow by a space-to-depth transformation. The neighboring frames are warped by the LR optical flow to make the neighboring frames align with the target frame. Then the super-resolution network (SRnet) takes the target frame and warped frames as inputs to obtain the final super-resolution result. SRnet consists of two convolutional layers, five residual dense blocks and a sub-pixel convolutional layer.

⁵Code: <https://github.com/LongguangWang/SOF-VSR>

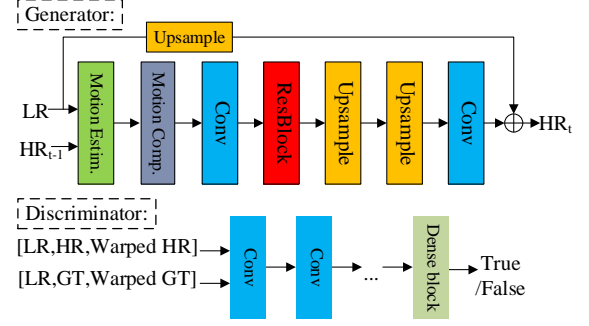


Fig. 12: The network architecture of TecoGAN [27].

9) *TecoGAN*: Temporally coherent GAN (TecoGAN)⁶ [27] mainly proposes a spatio-temporal discriminator for realistic and coherent video super-resolution, and a novel “Ping-Pong” loss to tackle recurrent artifacts. Like GAN, TecoGAN also consists of a generator and a discriminator and its architecture is shown in Fig. 12.

The generator takes the target frame, the previous frame and previous estimated HR frame as inputs. Firstly, input frames are fed into the optical flow module, which is a CNN similar to the optical flow estimation module in FRVSR [24]. In this module, the LR optical flow between the target frame and the neighboring frame is estimated and enlarged by the bicubic interpolation to attain the corresponding HR optical flow. Then the previous HR frame is warped by the HR optical flow. The warped previous HR frame and target frame are fed into subsequent convolutional modules that include two convolutional layers, a residual block and two upsample modules with the deconvolution layer, to yield a restored target frame. Moreover, the discriminator assesses the quality of super-resolution results. The discriminator takes the generated results and GT as inputs, where each of them has three components, that is, three consecutive HR frames, three corresponding upsampled LR frames and three warped HR frames. With such input formats, the spatial over-smooth and temporal inconsistency in the final results can be relieved. In addition, TecoGAN also proposes a “ping-pong” loss function to reduce the long-term temporal detail drift and make super-resolution results more natural.

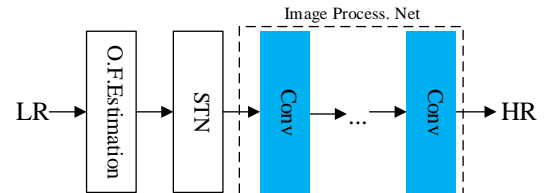


Fig. 13: The network architecture of TOFlow [28]. Here O.F. Estimation is the optical flow estimation, STN is a spatial transformer network, and Image Process. Net is an image processing network.

⁶Code: <https://github.com/thunil/TecoGAN>

10) *TOFlow*: The architecture of the task-oriented flow (TOFlow)⁷ [28] is shown in Fig. 13. TOFlow combines the network for optical flow estimation with the reconstruction network, and trains them jointly to obtain optical flow network tailored to a specific task such as video SR, video interpolation and video deblurring.

TOFlow adopts SpyNet [65] as the network for the optical flow estimation, and then adopts a spatial transformer network (STN) to warp the neighboring frame according to the computed optical flow. Then the final result is obtained by an image processing network. For the video super-resolution task, the image processing module consists of 4 convolutional layers, where kernel sizes are 9×9 , 9×9 , 1×1 , and 1×1 , respectively, and the numbers of channels are 64, 64, 64, and 3, respectively.

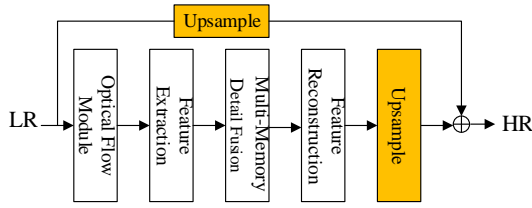


Fig. 14: The network architecture of MMCNN [29].

11) *MMCNN*: The architecture of the multi-memory convolutional neural network (MMCNN)⁸ [29] is shown in Fig. 14, and it consists of 5 major modules: optical flow module for motion estimation and motion compensation, feature extraction, multi-memory detail fusion, feature reconstruction, and upsample modules, where the last module uses a sub-pixel convolutional layer.

Consecutive input frames are first processed by the optical flow estimation module to make neighboring frames align with the target frame and then the warped frames are fed into subsequent network modules to attain the residual image of the target frame. Finally, this residual image is added into the upsampled LR target frame, which is computed by bicubic interpolation, to obtain the super-resolution result. In the multi-memory detail fusion module, MMCNN adopts the ConvLSTM module [70] to merge the spatio-temporal information. Moreover, the feature extraction, detail fusion, and feature reconstruction modules are all built based on residual dense blocks [57, 72], where the key difference of them only is the type of network layers.

12) *RBPN*: The recurrent back-projection network (RBPN)⁹ [30] is inspired by the back-projection algorithm [73, 74, 75]. RBPN mainly consists of one feature extraction module, a projection module, and a reconstruction module, and its architecture is shown in Fig. 15.

The feature extraction module includes two operations: One is to extract the features of the target frame, and the other is to extract the feature from the concatenation of the target frame, the neighboring frame, and

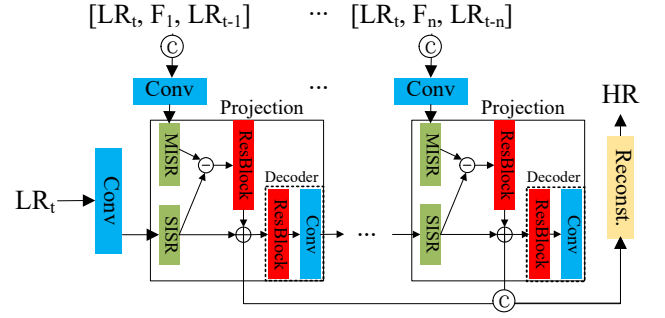


Fig. 15: The network architecture of RBPN [30], where \otimes denotes concatenation, \ominus is element subtraction, and MISR denotes multi-image super-resolution.

the calculated optical flow which is from the neighboring frame to the target frame, and then perform alignment implicitly. The optical flow is obtained by the pyflow¹⁰ method. The projection module consists of an encoder and a decoder. The encoder is composed of a multiple image super-resolution (MISR), a single image super-resolution (SISR) and residual blocks (denoted as ResBlock). The decoder consists of ResBlock and a strided convolution, and it takes the output of the previous encoder as input to produce LR features for the encoder of the next projection module. The concatenation of the target frame, the next neighboring frame and pre-computed optical flow are input to the feature extraction module, whose output is also for the encoder in the next projection module. The above process does not stop until all neighboring frames are processed. That is, projection is used recurrently, which is the reason of the words “recurrent back-projection network”. Finally, the reconstruction module takes the output of the encoder in each projection module by the mean of concatenation as input to produce the final SR result.

13) *MEMC-Net*: The motion estimation and motion compensation network (MEMC-Net)¹¹ [31], as shown in Fig. 16, mainly proposes an adaptive warping layer.

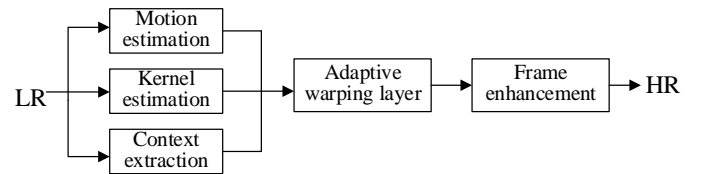


Fig. 16: The network architecture of MEMC-Net [31].

The adaptive warping layer warps the neighboring frame through the estimated optical flow and the convolutional kernel, which are resulted from a motion estimation network and a kernel estimation network, respectively, and aligns the neighboring frame with the target frame. The motion estimation network adopts FlowNet [61], and the kernel estimation network uses an improved U-Net [71] including five max-pooling layers,

⁷Code: <https://github.com/anchen1011/toflow>

⁸Code: <https://github.com/psychopa4/MMCNN>

⁹Code: <https://github.com/alterzero/RBPN-PyTorch>

¹⁰<https://github.com/pathak22/pyflow>

¹¹Code: <https://github.com/baowenbo/MEMC-Net>

five un-pooling layers and skip connections from the encoder to the decoder. In MEMC-Net, the architecture of the super-resolution module, namely frame enhancement module, is similar to that of EDSR [76]. In order to deal with the occlusion problem, it adopts a pre-trained ResNet18 [77] to extract the feature of input frames. Moreover, it feeds the output of the first convolutional layer of ResNet18 as the context information into the adaptive warping layer to perform the same operation.

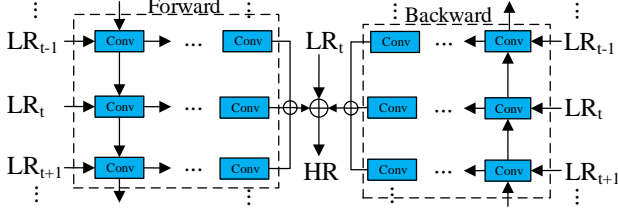


Fig. 17: The network architecture of RRCN [32].

14) *RRCN*: The residual recurrent convolutional network (RRCN) [32], as shown in Fig. 17, is a bidirectional recurrent neural network, which learns a residual image. RRCN proposes an unsynchronized full recurrent convolutional network, where unsynchronization refers to the input of multiple consecutive video frames, and only the middle one is super-resolved.

RRCN uses the combined local-global with total variable (GLG-TV) method [63] to perform motion estimation and compensation for the target frame and its adjacent frames. The compensated frames are used as input to the network. The forward convolution and recurrent convolution are conducted in the forward network and the backward network, respectively, and their outputs are summed up. Finally, the result is obtained by adding the target frame to the input. In order to further improve the performance, RRCN also uses the self-ensemble strategy and combines it with the output of the single image super-resolution method, EDSR+ [76], to obtain two models named RRCN+ and RRCN++, respectively.

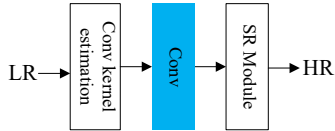


Fig. 18: The network architecture of RTVSR [33]. Here SR Module denotes super-resolution module.

15) *RTVSR*: The real-time video super-resolution (RTVSR) [33], as shown in Fig. 18, adopts a convolutional network called motion convolutional kernel estimation network, which is a full convolution codec structure, to estimate the motion between the target frame and the neighboring frame and produce a pair of 1D convolutional kernel corresponding to the current target frame and neighboring frame. Then the neighboring frame is warped by using estimated convolutional kernels to make it align with the target frame. RTVSR designs an

important component called gated enhance units (GEUs) to learn useful features, which is an improved variant based on [78].

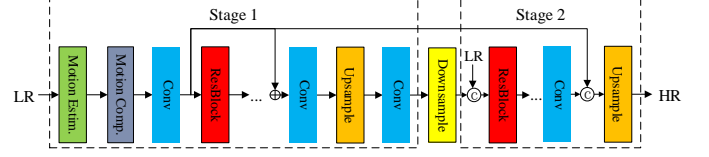


Fig. 19: The network architecture of MultiBoot VSR [34].

16) *MultiBoot VSR*: The multi-stage multi-reference bootstrapping for video super-resolution (MultiBoot VSR) [34] consists of two stages. That is, in order to further improve performance, the output of the first stage is used as the input of the second stage. The network architecture of MultiBoot VSR is shown in Fig. 19.

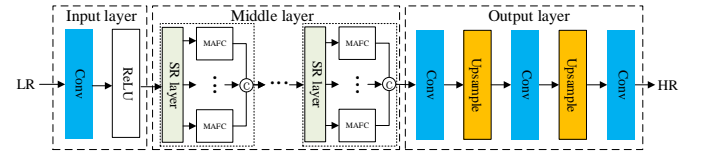


Fig. 20: The network architecture of MAFN [35].

17) *MAFN*: The architecture of motion-adaptive feedback network (MAFN) [35] is shown in Fig. 20. MAFN consists of three parts: an input layer to map input frames into the deep features, a mid layer to convert the features to more complete facial features, and an output layer to produce the output image from the facial presentation features. With the feature map from the input layer, each submodule in mid layer updates the representation features of each input by a simple super-resolution layer (SR layer) consisting of two convolutional layers and a ReLU layer. Then, the adjacent features are used as the inputs and sent to the Motion-Adaptive Feedback Cell (MAFC) in pairs for generating the corresponding motion compensation information. Finally, the motion compensation information is combined with the newly obtained representation features to yield the final output.

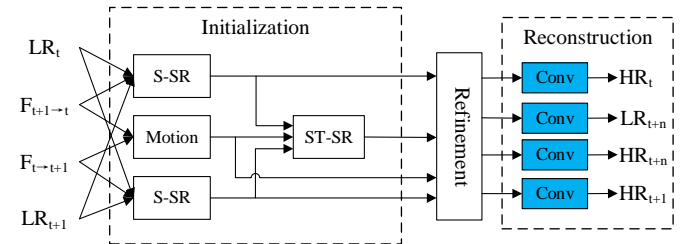


Fig. 21: The network architecture of STARnet [36].

18) *STARnet*: The architecture of space-time-aware multi-resolution networks (STARnet) [36] is shown in Fig. 21. STARnet is an end-to-end network that can simultaneously process video super-resolution and video

interpolation. It consists of the following three stages: initialization, refinement and reconstruction.

In the initialization stage, STARnet receives four parts of inputs including two LR RGB frames and their bi-directional flow images. In this stage, the two spatial super-resolution (S-SR) modules can execute super-resolution to the two LR frames by DBPN [75] or RBP [30] and re-generate their LR counterparts by a similar network to prepare for frame interpolation in both LR and HR spaces in the spatio-temporal super-resolution (ST-SR) module. Meanwhile, the motion module aligns the bi-directional flow images.

In summary, MEMC techniques are used to align neighboring frames with the target frame, which is the most common method for solving the video super-resolution problem. However, the problem is that they cannot guarantee the accuracy of motion estimation when the lighting changes dramatically or there are large motions in videos. In these cases, the performance of the video super-resolution degrades greatly. To address this issue, the methods with alignment, e.g., the deformable convolution which is presented as one module in the deep network to align frames, and the methods without alignment are both proposed.

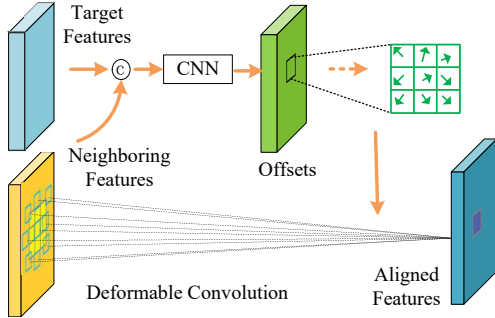


Fig. 22: Deformable convolution used for frame alignment.

B. Deformable Convolution Methods

The deformable convolutional network was first proposed by Dai et al. [79] in 2017 and the improved variant [80] was proposed in 2019. In ordinary CNNs, the convention is to use a fixed geometric structure in a layer, which restricts the network's capability to model geometric transformations. In contrast, the deformable convolution is able to overcome this limitation. The illustration of the deformable convolution for feature alignment is shown in Fig. 22. The target feature maps concatenating with the neighboring feature maps are projected to attain offsets via additional convolutional layers. The offsets are applied to the conventional convolution kernel to yield a deformable convolution kernel, and then it is convolved with the input feature maps to produce the output feature maps. The methods that adopt deformable convolution mainly include the enhanced deformable video restoration (EDVR) [37], de-

formable non-local network (DNLN) [38], and temporally deformable alignment network (TDAN) [39], which are depicted in detail as follows.

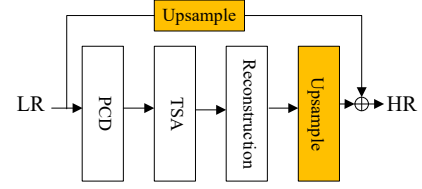


Fig. 23: The network architecture of EDVR [37], where PCD is the pyramid, cascading and deformable alignment module, and TSA is the temporal-spatial attention fusion module.

1) *EDVR*: The enhanced deformable video restoration (EDVR)¹² [37], as shown in Fig. 23, is the champion model in the NTIRE19 Challenge [81, 82]. EDVR proposes two key modules: the pyramid, cascading and deformable (PCD) alignment module as in [65, 83, 84, 85] and the temporal-spatial attention (TSA) fusion module, which are used to solve large motions in videos and to effectively fuse multiple frames, respectively.

EDVR mainly consists of four parts: one PCD alignment module, a TSA fusion module, a reconstruction module, and an upsample module using a sub-pixel convolutional layer. Firstly, the input frames are aligned by the PCD alignment module, and then the aligned frames are fused by the TSA fusion module. Then the fused results are fed into the reconstruction module to refine the features, and then through the up-sampling, a HR image called the residual image is obtained. The final result is obtained by adding the residual image to a direct upsampling target frame. To further improve performance, EDVR also adopts a two-phase approach, whose second phase is similar to the first but with a shallower network depth.

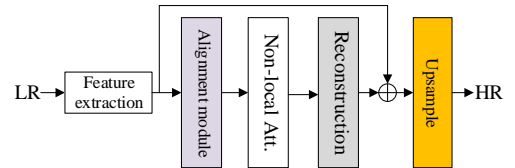


Fig. 24: The network architecture of DNLN [38]. Here Non-local Att. is the non-local attention module.

2) *DNLN*: The deformable non-local network (DNLN)¹³ [38], as shown in Fig. 24, designs an alignment module and a non-local attention module based on the deformable convolution [79, 80] and non-local networks [86], respectively. The alignment module uses the hierarchical feature fusion module (HFFB) [87] within the original deformable convolution to generate convolutional parameters. Moreover, DNLN

¹²Code: <https://github.com/xinntao/EDVR>

¹³Code: <https://github.com/wh1h/DNLN>

utilizes multiple deformable convolutions in a cascaded way, which makes inter-frame alignment more accurate.

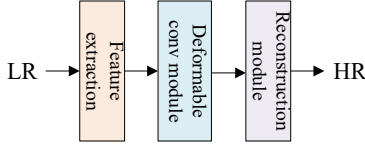


Fig. 25: The network architecture of TDAN [39].

3) *TDAN*: The temporally deformable alignment network (TDAN)¹⁴ [39], as shown in Fig. 25, applies deformable convolution to the target frame and the neighboring frame, and attains corresponding offsets. Then the neighboring frame is warped in terms of the offsets to align with the target frame. TDAN is divided into three parts, i.e., a feature extraction module, a deformable convolution module and a reconstruction module.

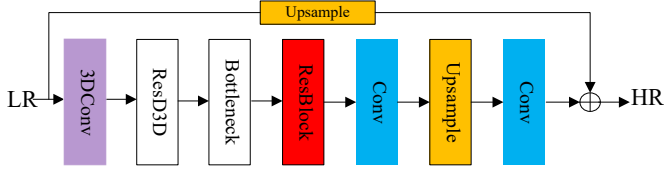


Fig. 26: The network architecture of D3Dnet [40].

4) *D3Dnet*: The architecture of the deformable 3D convolution network (D3Dnet)¹⁵ [40] is shown in Fig. 26. D3Dnet proposes 3D deformable convolution to achieve strong spatio-temporal feature modeling capability. The inputs are first fed to a 3D convolutional layer to generate features, which are then fed to 5 Residual Deformable 3D Convolution (ResD3D) blocks to achieve motion compensation and capture spatial information.

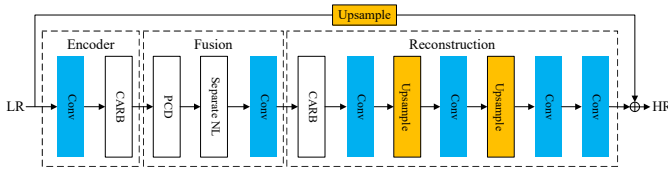


Fig. 27: The architecture of VESR-Net [41], where CARB is the channel-attention residual block, and Separate NL denotes the separate non-local architecture.

5) *VESR-Net*: The architecture of video enhancement and super-resolution network (VESR-Net) [41], as shown in Fig. 27, is the champion model in the Youku video enhancement and super-resolution challenge. VESR-Net mainly consists of a feature encoder, a fusion module and a reconstruction module.

The LR frames are firstly processed by the feature encoder consisting of a convolution layer and several stacked channel-attention residual blocks (CARBs) [58]. Then in the fusion module, the PCD convolution in [37]

performs the inter-frame feature alignment. The separate non-local submodule (Separate NL) divides feature maps in spatial, channel and temporal dimensions and processes them to obtain correlation information separately. In contrast to the vanilla non-local [86] architecture, Separate NL can fuse the information across video frames and across pixels in each frame with less parameters and shallower network. Finally, VESR-Net utilizes CARBs followed with a feature decoder for upsampling in the reconstruction module, where the upsample module is implemented by a sub-pixel convolutional layer. And it outputs the super-resolved frame by adding with the bicubic-interpolation LR target frame.

The evolution of methods with alignment. In the methods with alignment, the motion estimation and motion compensation techniques, as a classic research topic in computer vision, have been applied to video super-resolution in the early years. MEMC has wide range of applications such as video coding and enhancing the interlaced scanning. As the advent of deep learning based VSR, many works employ MEMC to capture the motion information between frames. The early work of MEMC is Deep-DE [19], and some recently proposed methods such as VESPCN [21], SOFVSR [26], TOFlow [28] and FRVSR [24] also adopted MEMC techniques. Specifically, early video super-resolution algorithms adopt traditional MEMC methods such as Druleas in VSRnet [20], while subsequent algorithms such as VESPCN [21], TOFlow [28] and FRVSR [24] mainly design sub-module or sub-network for MEMC.

However, the accuracy of most MEMC methods is usually not guaranteed. When the luminance changes or the videos contain large motions between frames, the VSR performance degrades dramatically. Hence, the deformable convolution, which is not sensitive to varying lighting and motion conditions, has attracted more attention from researchers. The deformable convolution was proposed by Dai et al. [79] for enhancing the transformation modeling capability of CNNs for the geometric variations of objects. In the VSR methods, TDAN [39] first utilized it to perform inter-frame alignment. After that, DNLN [38], EDVR [37], STVSR [88] and D3Dnet [40] further promote it for frame alignment. Nevertheless, the deformable convolution still has some drawbacks including high computational complexity and harsh convergence conditions. Therefore, the technique has room for further improvement in future research works.

V. METHODS WITHOUT ALIGNMENT

In contrast to the methods with alignment, the methods without alignment do not align neighboring frames for video super-resolution. This type of methods mainly exploit the spatial or spatio-temporal information for feature extraction. We further categorize them into four main types: the 2D convolution methods (2D Conv), 3D convolution methods (3D Conv), recurrent convolutional neural network (RCNN), and non-local network based

¹⁴Code: <https://github.com/YapengTian/TDAN-VSR-CVPR-2020>

¹⁵Code: <https://github.com/XinyiYing/D3Dnet>

methods. Among them, the first type falls into the spatial methods, while the other three are the spatio-temporal methods, whose characteristic is to exploit both the spatial and temporal information from input videos. The differences are the utilized dominating techniques. We present them in detail as follows.

A. 2D Convolution Methods

Instead of alignment operations such as motion estimation and motion compensation between frames, the input frames are directly fed into a 2D convolutional network to spatially perform feature extraction, fusion and super-resolution operations. This may be a simple approach for solving the video super-resolution problem since it makes the network learn the correlation information within frames by itself. The representative methods are VSRResFeatGAN [42] and FFCVSR [43].

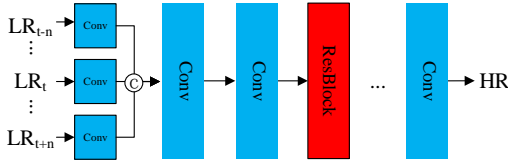


Fig. 28: The architecture of the generator in VSRResFeatGAN [42].

1) *VSRResFeatGAN*: VSRResFeatGAN [42] utilizes GAN to address VSR tasks and find a good solution by adversarial training. The generator shown in Fig. 28 consists of convolutional layers and residual blocks. And each residual block is composed of two convolutional layers and is followed by a ReLU activation function. Moreover, the discriminator consists of three groups of convolutions and a fully connected layer, where each group includes a convolutional layer, Batch Normalization (BN), and LeakyReLU. The discriminator determines whether the output of the generator is a generated image or GT image. Then the result of the discriminator reacts to the generator, and promotes it to yield results closer to the GT images. Finally, a relative satisfactory solution is obtained through an iterative optimization.

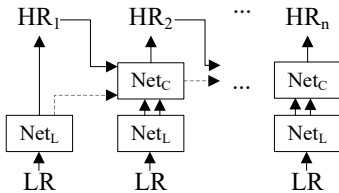


Fig. 29: The architecture of FFCVSR [43]. Here Net_C is the context network, and Net_L is the local network.

2) *FFCVSR*: The architecture of the frame and feature-context video super-resolution (FFCVSR)¹⁶ [43] is shown in Fig. 29. Unlike common MEMC techniques, FFCVSR consists of several local networks and context networks

and utilizes inter-frame information in a different way. The LR unaligned video frames and the HR output of the previous frame are directly taken as inputs to the network for the purpose of restoring high-frequency details and maintaining temporal consistency.

In summary, the above two methods both exploit spatial correlation between frames for VSR tasks. VSRResFeatGAN utilizes adversarial training of GANs to find an appropriate solution. As the discriminator in GANs has to guess whether the generated frame is close to the ground truth, the VSR results in terms of PSNR and SSIM are not always satisfactory compared with other methods, such as FFCVSR.

B. 3D Convolution Methods

The 3D convolutional module [89, 90] operates on spatio-temporal domain, compared with 2D convolution, which only utilizes spatial information through the sliding kernel over input frame. This is beneficial to the processing of video sequences, as the correlations among frames are considered by extracting temporal information. The representative 3D convolution methods for VSR are DUF [44], FSTRN [45], and 3DSRnet [46].

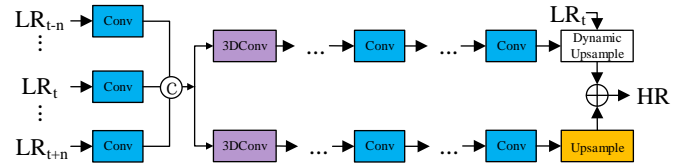


Fig. 30: The network architecture of DUF [44].

1) *DUF*: The dynamic upsampling filters (DUF)¹⁷ [44] has been proposed, as shown in Fig. 30. It is inspired by the dynamic filter network [91] that can generate corresponding filters for specific inputs and then apply them to generate corresponding feature maps.

The structure of the dynamic up-sampling filter, together with the spatio-temporal information learned by 3D convolution, can avoid the use of motion estimation and motion compensation. DUF performs not only filtering, but also the up-sampling operation. In order to enhance high frequency details of the super-resolution result, DUF uses a network to estimate residual map for the target frame. The final result is the sum of the residual map and the LR target frame processed by the dynamic upsample module with learned filters.

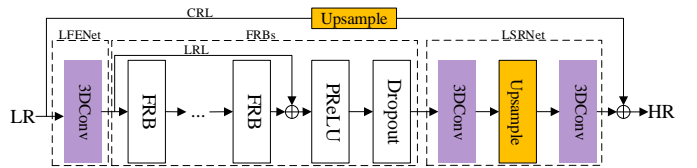


Fig. 31: The network architecture of FSTRN [45]. Here FRB denotes the fast spatio-temporal residual block.

¹⁶Code: <https://github.com/linchuming/FFCVSR>

¹⁷Code: <https://github.com/yhjo09/VSR-DUF>

2) *FSTRN*: The fast spatio-temporal residual network (FSTRN) [45] uses a factorized 3D convolution to extract information among consecutive frames, as shown in Fig. 31. In FSTRN, a $k \times k \times k$ 3D convolutional kernel is decomposed into 2 cascaded kernels, whose sizes are $1 \times k \times k$ and $k \times 1 \times 1$, respectively, to reduce the computation caused by directly using the 3D convolution.

FSTRN consists of the following four parts: an LR video shallow feature extraction net (LFENet), fast spatio-temporal residual blocks (FRBs), an LR feature fusion and up-sampling SR net (LSRNet), and a global residual learning (GRL) module. LFENet using 3D convolution to extract features for consecutive LR input frames. FRBs, including the decomposed 3D convolutional layers, are responsible for extracting spatio-temporal information among input frames. LSRNet is used to fuse information from previous layers and conducting up-sampling.

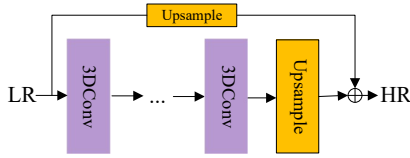


Fig. 32: The network architecture of 3DSRNet [46].

3) *3DSRnet*: The 3D super-resolution network (3DSRNet)¹⁸ [46] uses 3D convolution to extract spatio-temporal information among consecutive video frames for VSR tasks. The network architecture is shown in Fig. 32. 3DSRNet proposes an approach for scene change in practical applications, where a shallow network is proposed to judge input consecutive frames. If the scene change is detected in the current frame, it will be replaced by the frame that has the same scene and is the closest to current frame. The substituted sequences will be sent to the subsequent video super-resolution network. This approach overcomes performance degradation caused by scene change to some extent.

In brief, these 3D convolutional methods can extract spatio-temporal correlations among consecutive frames, rather than perform the motion estimation to extract motion information among frames and motion compensation to align them. However, most of the methods have relatively higher computational complexities compared with those of 2D convolutional methods, which limits them for real-time video super-resolution tasks.

C. Recurrent Convolutional Neural Networks (RCNNs)

It is well known that RCNNs have strong power of temporal dependency in modeling sequential data processing, e.g., natural language, video and audio. A straightforward way is to use RCNNs to handle video sequences. Based on this key idea, several RCNN methods such as BRCN [47, 48], STCN [49], and RISTN [50] have been proposed for video super-resolution.

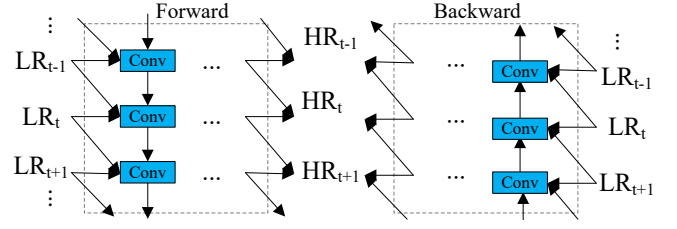


Fig. 33: The network architecture of BRCN [47, 48].

1) *BRCN*: The bidirectional recurrent convolutional network (BRCN) [47, 48], as shown in Fig. 33, is composed of two modules: a forward sub-network and a backward one with a similar structure, which only differ in the order of processing sequence. The forward subnet is responsible for modeling the temporal dependency from previous frames, while the backward subnet models temporal dependency from subsequent frames.

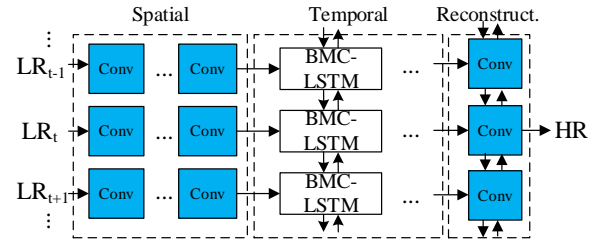


Fig. 34: The network architecture of STCN [49]. Here BMC denotes the bidirectional multi-scale convolution.

2) *STCN*: The spatio-temporal convolutional network (STCN) [49] is an end-to-end VSR method without MEMC, as shown in Fig. 34. The temporal information within frames is extracted by using LSTM [92]. Similar to RISTN [50], the network consists of three parts: a spatial module, a temporal module and a reconstruction module. Spatial module is responsible for extracting features from multiple consecutive LR frames. Temporal module, is a bidirectional multi-scale convoluted variant of LSTM, and is designed for extracting temporal correlation among frames.

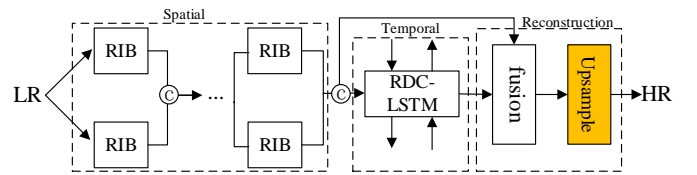


Fig. 35: The network architecture of RISTN [50], where RIB denotes the residual invertible block, and RDC is the residual dense convolution.

3) *RISTN*: The residual invertible spatio-temporal network (RISTN)¹⁹ [50] is inspired by the invertible block [93]. As shown in Fig. 35, it designs a residual invertible block (RIB), a LSTM with residual dense convolution (RDC-LSTM), and a sparse feature fusion strategy to

¹⁸Code: <https://github.com/sooyekim/3DSRnet>

¹⁹Code: <https://github.com/lizhuangzi/RISTN>

adaptively select useful features. Here RIB is used to extract spatial information of video frames effectively, and RDC-LSTM is used to extract spatio-temporal features.

The network is mainly divided into three parts: a spatial module, a temporal module and a reconstruction module. The spatial module is mainly composed of multiple parallel RIBs, and its output is used as the input of the temporal module. In the temporal module, after extracting spatio-temporal information, features are selectively fused by a sparse fusion strategy. Finally, the HR result of the target frame is reconstructed by the deconvolution in the reconstruction module.

In summary, RCNN-based methods are suitable for modeling the spatio-temporal information in videos, since they can map neighboring frames and thus effectively establish long-term dependence with more lightweight structures. However, conventional RCNN-based methods are difficult to train and sometimes suffer from the gradient vanishing problem. And they may not capture long-term dependence when the length of input sequences is too large, and thus may not achieve great performance. While LSTM-based methods can overcome these constraints to some extent with the help of the memorization of features from shallower layers. However, the complex design of LSTM is a factor that limits their depth on hardware, restraining them to model very long-term dependence.

D. Non-Local Methods

The non-local-based method is another one that utilizes both spatial and temporal information in video frames for super-resolution. This method benefit from the key idea of the non-local neural network [86], which was proposed to capture long-range dependencies for video classifications. It overcomes the flaws that convolution and recurrent computations are limited to the local area. Intuitively, a non-local operation is to calculate the response value of a position, which is equal to the weight sum of all possible positions in the input feature maps. Its formula is given as follows:

$$y_i = \frac{1}{\mathcal{C}(x)} \sum_{\forall j} f(x_i, x_j) g(x_j) \quad (6)$$

where i is the index of the output location where the response value needs to be calculated, j is the index of all possible locations, x and y are the input and output data with the same dimensions, f is a function to calculate the correlation between i and j , g is the function which calculates the feature representation of input data and $\mathcal{C}(x)$ is the normalization factor. Here, g is usually defined as: $g(x_j) = W_g x_j$, where W_g is the weight matrix that needs to learn. It should be noted that f has multiple choices such as Gaussian, dot product, and concatenation. Therefore, the non-local block can easily be added into existing deep CNNs.

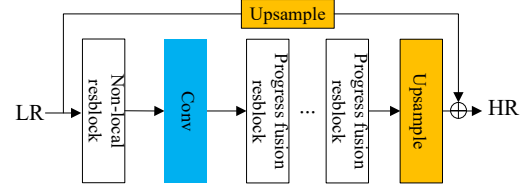


Fig. 36: The network architecture of PFNL [51].

1) *PFNL*: The progressive fusion non-local (PFNL) [51] method is illustrated in Fig. 36. It mainly includes three parts: a non-local resblock, progressive fusion residual blocks (PFRB) and an upsampling block.

PFNL uses non-local residual blocks to extract spatio-temporal features, and PFRB is proposed to fuse them. Finally, the output through a sub-pixel convolutional layer is added to the input frame that is up-sampled by the bicubic interpolation, which is the final super-resolution result. PFRB is composed of three convolutional layers. Firstly, the input frames are convoluted with the 3×3 kernels, respectively, then the output feature maps are concatenated, and the channel dimension is reduced by performing the 1×1 convolution. And the results are concatenated with the previous convoluted feature maps, respectively, and conducted with a 3×3 convolution. The final results are added to each input frame to obtain the output for current PFRB.

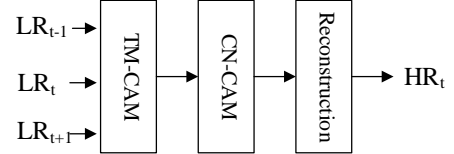


Fig. 37: The network architecture of MuCAN [52].

2) *MuCAN*: The architecture of multi-correspondence aggregation network (MuCAN) [52] is shown in Fig. 37. MuCAN is an end-to-end network consisting of a temporal multi-correspondence aggregation module (TM-CAM), a cross-scale non-local-correspondence aggregation module (CN-CAM), and a reconstruction module.

In TM-CAM, two neighboring LR frames are first encoded into lower resolutions features to be more stable and robust to noise. Then the aggregation starts in the original LR feature space by an aggregation unit (AU) to compensate large motion while progressively moving up to low-level/high-resolution stages for subtle sub-pixel shift. In a single AU, a patch-based matching strategy is used since it naturally contains structural information. Multiple candidates are then aggregated to obtain sufficient context information. The aggregated information is then passed to CN-CAM, which then uses a pyramid structure based on AvgPool to execute spatio-

²¹UVGD denotes the Ultra Video Group Database

²²LMT denotes the LIVE video quality assessment database, the MCL-V database, and the TUM 1080p dataset.

²³REDS denotes the REalistic and DIverse Scenes

TABLE II: Some widely used video super-resolution datasets. Note that ‘-’ represents unknown information.

Dataset	Year	Type	Download Link	Video Number	Resolution	Color Space
YUV25	-	Train	https://media.xiph.org/video/derf/	25	386×288	YUV
TDTF	-	Test	www.wisdom.weizmann.ac.il/~vision/SingleVideoSR.html	5	648×528 for Turbine, 960×530 for Dancing, 700×600 for Treadmill, and 1000×580 for Flag, 990×740 for Fan	YUV
Vid4	2011	Test	https://drive.google.com/drive/folders/10-gUO6zBeOpWEamrWKCtSkkUFukB9W5m	4	720×480 for Foliage and Walk, 720×576 for Calendar, and 704×576 for City	RGB
YUV21	2014	Test	http://www.codersvoice.com/a/webbase/video/08/152014/130.html	21	352×288	YUV
Venice	2014	Train	https://www.harmonicinc.com/free-4k-demo-footage/	1	$3,840 \times 2,160$	RGB
Myanmar	2014	Train	https://www.harmonicinc.com/free-4k-demo-footage/	1	$3,840 \times 2,160$	RGB
CDVL	2016	Train	http://www.cdvl.org/	100	$1,920 \times 1,080$	RGB
UVGD ²¹	2017	Test	http://ultravideo.cs.tut.fi/	7	$3,840 \times 2,160$	YUV
LMT ²²	2017	Train	http://mcl.usc.edu/mcl-v-database/ , http://live.ece.utexas.edu/research/quality/live_video.html , https://vision.in.tum.de/data/datasets	-	$1,920 \times 1,080$	RGB
Vimeo-90K	2019	Train+Test	http://toflow.csail.mit.edu/	91,701	448×256	RGB
REDS ²³	2019	Train+Test	https://seungjunnah.github.io/Datasets/reds.html	270	$1,280 \times 720$	RGB

TABLE III: Some major video super-resolution competitions. Note that ‘EDVR+’ stands for a method based on EDVR, and ‘-’ represents unknown information.

Name	Year	Organizer	Location	Website	Dataset	Scale	Champion	PSNR	SSIM
NTIRE 2019 Video Restoration and Enhancement Challenges	2019	CVPR	Long Beach, California	https://data.vision.ee.ethz.ch/cv1/ntire19/	REDS	$\times 4$	EDVR [37]	31.79	0.8962
YOUKU Video Super-Resolution and Enhancement Challenge	2019	Alibaba	Hangzhou, China	https://tianchi.aliyun.com/competition/entrance/231711/introduction	Youku-VESR	$\times 4$	VESR-Net [41]	37.85	-
AIM 2019 Challenge on Video Extreme Super-Resolution	2019	ECCV	Hong Kong, China	https://www.aim2019.org/	Vid3oC	$\times 16$	EDVR+	22.53	0.6400
Mobile Video Restoration Challenge	2019	ICIP & Kwai	-	https://www.kuaishou.com/activity/icip2019	-	-	-	-	-
AIM 2020 Challenge on Video Extreme Super-Resolution	2020	ECCV	Boston, Massachusetts	http://aim2020.org/	Vid3oC	$\times 16$	EVEsrNet [94]	22.83	0.6450

temporal non-local attention and coarse-to-fine spatial attention. Finally, the results are aggregated and sent to the reconstruction module to yield the final HR result.

In summary, the non-local based methods introduce attention mechanisms into VSR tasks. They can establish effective dependence of spatio-temporal information by extending the receptive field to the global. However, the non-local modules used in them need to calculate the response at each position by attending to all other positions and computing a weighted average of the features in all positions. Thus, this incurs high computational cost, and some efforts can be made to reduce the computational overhead of the methods.

Moreover, the methods without alignment rely on the non-linear capability of the neural network to learn the motion correlation between frames for video super-resolution. They do not utilize additional modules to

align frames. The learning ability largely depends on the design of the deep neural network. And an elaborate design is more likely leading to higher performance for video super-resolution.

VI. PERFORMANCE COMPARISONS

A. Datasets and Competitions

Details of some of the most popular datasets used in VSR tasks are summarized in Table II. The most widely-used dataset for training is Vimeo-90K, since it is currently the largest VSR dataset with real scenes. The most popular dataset for testing is Vid4, whose frames contain more high-frequency details than others. Thus, Vid4 is frequently used for evaluating the performance of VSR methods. REDS includes videos with extremely large movement, which is challenging for VSR methods.

Besides, we also summarize several international competitions on video super-resolution in Table III. The NTIRE 2019 Challenge aims at recovering videos with large movements and diverse real-world scenes. Its winning solution is EDVR [37], which may be the most popular work for VSR. The AIM Challenges in 2019 and 2020 both encourage solutions of VSR with large scale factors. A method enhanced from EDVR won the AIM 2019 Challenge, while EVESRNet [94] won the AIM 2020 Challenge. Besides, the YOUKU Video Super-Resolution and Enhancement Challenge, and Mobile Video Restoration Challenge in 2019 are both for videos which are more relevant to entertainment. The winning solution of YOUKU challenge is VESR-Net [41]. These competitions are making great contributions to the development of video super-resolution and helping develop new methods for various video super-resolution applications.

B. Performance of Methods

Moreover, we summarize the performance of the representative VSR methods with scale factor 4 in Table IV in terms of both PSNR and SSIM. More experimental results for VSR tasks with magnification factors 2 and 3 are reported in Supplementary Materials. The degradation types are the bicubic downsampling with the image-resize function (BI) and Gaussian blurring and downsampling (BD). Note that all the PSNR and SSIM are from their original works. And a simple comparison on the performance may not be fair, since the training data, the pre-processing, and the cropped area in videos are likely totally different in the methods.

According to Table IV, the top 3 methods in the $\times 4$ VSR task are EDVR, RBPN and FFCVSR. It is found that the newest VSR methods (e.g., EDVR and RBPN) have been verified efficient compared with earlier methods (e.g., VSRnet and VESPCN). This is likely due to development of deeper and more complex network structures, and thanks to the improvement of the computational ability of hardware. However, the performance of the latest methods still needs to be improved in the future.

It is clear that there are some common characteristics among the methods with superior performance. Similarly, the architectures of both MMCNN and RRCN include some recurrent structures, e.g., LSTM in MMCNN and the non-simultaneous recurrent structure of RRCN, which improve their robustness on high frequency details and dependence of long temporal distance. As for EDVR, RBPN and FFCVSR, they all contain some modules that jointly use features across layers like PCD alignment in EDVR, back-projection in RBPN and feature-context in FFCVSR. The modules can help remain temporal consistence and bring less artifacts and jams to the recovered results.

Furthermore, MEMC-based methods are more suitable for video super-resolution of generic videos, since they enjoy more stable performance and relatively less computational complexities. However, if the videos contain large motions, other alternative techniques can be

applied. For example, deformable convolution based methods are more suitable for applications close to the real scenes regardless of computational costs. Besides deformable convolution, some techniques like 3D convolution and non-local networks are also not suitable for real-time applications.

VII. TRENDS AND CHALLENGES

Although great progress has been made by state-of-the-art video super-resolution methods based on deep learning especially on some public benchmark datasets, there are still challenges and trends discussed below.

A. Lightweight Super-Resolution Models

The deep learning based video super-resolution methods though enjoy high performance, they have difficulty in deploying efficiently in many real-world problems. It is noted that their models usually have a mass of parameters and require vast computing and storage resources, and their training also takes a long time. With the popularity of mobile devices in modern life, one expects to apply these models on such devices. How to design and implement a lightweight super-resolution algorithm with high performance for real-world applicants is a major challenge.

B. Interpretability of Models

Deep neural networks are usually considered as black boxes. That is, we do not know what real information the model learns when the performance is good or bad. In existing video super-resolution models, there is not a theoretical interpretation about how convolution neural networks recover low-resolution video sequences. With a deeper investigation on its interpretation, the performance of super-resolution algorithms for both videos and images may be improved greatly.

C. Super-Resolution with Larger Scaling Factors

For video super-resolution tasks, existing works mainly focus on the case of the magnification factors $\times 2$, $\times 3$ and $\times 4$. The more challenging scales such as $\times 8$ and $\times 16$ have been rarely explored. With the popularity of high resolution (e.g., 8K and 16K) display devices, larger scaling factors are to be further studied. Obviously, as the scale becomes larger, it is more challenging to predict and restore unknown information in video sequences. This may result in performance degradation for the algorithms, and weaken robustness in the models. Therefore, how to develop stable deep learning algorithms for VSR tasks with larger scaling factors is still challenging.

TABLE IV: Comparison of all the methods on the datasets with scale factor $\times 4$. Noted that ‘Internet’ means that the dataset is collected from the internet. ‘*’ denotes that the source of the dataset is unknown, and ‘-’ indicates that the method does not be tested on the datasets.

Method	Training Set	Test Set	Scale	BI		BD	
				PSNR	SSIM	PSNR	SSIM
VSRnet [20]	Myanmar	Vid4	$\times 4$	24.84	0.7049	-	-
		Myanmar-T		31.85	0.8834	-	-
VESPCN [21]	CDVL	Vid4		25.35	0.7557	-	-
3DSRnet [46]	largeSet	Vid4		25.71	0.7588	-	-
MMCNN [29]	*	Vid4		26.28	0.7844	-	-
		Myanmar-T		33.06	0.9040	-	-
		YUV21		28.90	0.7983	-	-
		Vid4+temple+penguin		28.97	-	-	-
TOFlow [28]	Vimeo-90K	Vid4		-	-	23.54	0.8070
		Vimeo-90K-T		-	-	33.08	0.9417
TecoGAN [27]	*	ToS		-	-	32.75	-
		Vid4		-	-	25.89	-
MultiBoot [34]	REDS	REDS-T		31.00	0.8822	-	-
Deep-DE [19]	*	city+temple+penguin		-	-	29.00	0.8870
SOFVSR [26]	CDVL	DAVIS-10		34.32	0.9250	-	-
		Vid4		26.01	0.7710	-	-
MEMC-Net [31]	Vimeo-90K	Vimeo-90K-T		33.47	0.9470	-	-
		Vid4		24.37	0.8380	-	-
FRVSR [24]	vimeo.com	Vid4		-	-	26.69	0.8220
RBPN [30]	Vimeo-90K	Vid4		27.16	0.8190	-	-
		SPMCS		30.10	0.8740	-	-
DRVSR [22]	*	Vid4		25.52	0.7600	-	-
		SPMCS		29.69	0.8400	-	-
FFCVSR [43]	Venice+Myanmar	Vid4		26.97	0.8300	-	-
VSRResNet [42]	Myanmar	Vid4		25.51	0.7530	-	-
MAFN [35]	VoxCeleb	VoxCeleb-T		-	-	34.59	0.9279
STARnet [36]	Vimeo-90K	UCF101		29.11	0.9240	-	-
		Vimeo-90K-T		30.83	0.9290	-	-
		Middlebury		27.16	0.8270	-	-
		Vid4		27.35	0.8264	-	-
EDVR [37]	Vimeo-90K	Vimeo-90K-T		37.61	0.9489	-	-
		REDS4		31.09	0.8800	28.88	0.8361
TDAN [39]	Vimeo-90K	Vid4		26.24	0.7800	26.58	0.801
D3Dnet [40]	Vimeo-90K	Vid4		26.52	0.799	-	-
VESR-Net [41]	Youku-VESR	Youku-VESR-T		-	-	35.97	-
DNLN [38]	Vimeo-90K	Vid4		-	-	27.31	0.8257
		SPMCS		-	-	30.36	0.8794
RVSR [23]	LMT	Vid4+temple+penguin		28.05	-	-	-
		UVGD		39.71	-	-	-
FSTRN [45]	YUV25	TDTEF		-	-	29.95	0.8700
BRCN [48]	YUV25	Vid4		-	-	24.43	0.6334
		TDTEF		-	-	28.20	0.7739
RRCN [32]	Myanmar	Myanmar-T		32.35	0.9023	-	-
		Vid4		25.86	0.7591	-	-
		YUV21		29.08	0.7986	-	-
DUF [44]	Internet	Vid4		-	-	26.81	0.8145
PFNL [51]	*	Vid4		-	-	27.40	0.8384
MuCAN [52]	Vimeo90K+REDS	REDS4		30.88	0.8750	-	-
		Vimeo-90K-T		35.49	0.9344	-	-
STCN [49]	*	Hollywood2		-	-	34.58	0.9259
		city+temple+penguin		-	-	30.27	0.9103

D. Super-Resolution with Random Scaling Factors

According to Table IV, most video super-resolution methods are designed for the case of the scaling factor $\times 4$ in default, which is not appropriate for real scenes. On the one hand, other scales like $\times 2$, $\times 3$ or $\times 1.5$ are also very common in VSR tasks. On the other hand, a video super-resolution model with fixed scale will seriously limit its generalization and portability. Therefore, a universal VSR method for arbitrary scale factors is greatly needed in real-world applications.

E. More Reasonable & Proper Degradation Process of Videos

In existing works, the degraded LR videos are attained through the two methods: One is directly downsampling HR videos by using interpolation, such as bicubic. The other is performing the Gaussian blurring on HR videos and then downsampling the video sequences. Although both methods perform well in theory, they always act poorly in practice. As it is known, the real-world degradation process is very complex and includes much uncertainty. The blurring and interpolation are not adequate for modeling the problem. Therefore, when constructing LR videos, the degradation should be mod-

eled theoretically in consistent with the real-world case to reduce the gap between research and practice.

F. Unsupervised Super-Resolution Methods

Most state-of-the-art VSR methods adopt supervised learning. The deep neural networks require a large number of paired LR and HR video frames for training. However, such paired datasets are hard or costly to obtain in practice. One may synthesize the LR/HR video frames, the performance of super-resolution methods is still not satisfied as the degradation model is too simple to characterize the real-world problem and results in inaccurate HR/LR datasets. Thus, unsupervised VSR methods are highly demanded.

G. More Effective Scene Change Algorithms

Existing video super-resolution methods rarely involve the videos with scene change. In practice, a video sequence usually has many different scenes. When we consider the problem of video super-resolution on such videos, they have to be split into multiple segments without scene change and process individually. This may result in large computational time. Therefore, deep learning methods that can process videos with scene change are necessary for real-world applications.

H. More Reasonable Evaluation Criteria for Video Quality

The criterion for evaluating the quality of super-resolution results mainly includes PSNR and SSIM. However, their values are not able to reflect the video quality for human perception. That is, even if the PSNR value of a video is very high, the video is uncomfortable for human. Therefore, new video evaluation criteria that are consistent with human perception need to be developed. Some evaluation criteria have been proposed, nevertheless, more criteria which can be broadly accepted are still needed.

I. More Effective Methods for Leveraging Information

An important characteristic of video super resolution is leveraging the information among frames. Whether the utilization is effective or not influences the performance directly. Although many methods have been proposed as mentioned in this paper, there are still some disadvantages. For instance, 3D convolution and non-local modules have a large amount of computation, and the accuracy of optical estimation can not be guaranteed. Therefore, the methods that can effectively utilize information among frames is worth further studying.

VIII. CONCLUSIONS

In this paper, we reviewed the development of deep learning approached for video super-resolution in recent years. We first classified existing video super-resolution algorithms by the way of leveraging information within

frames. Then we found that although video super-resolution algorithms based on deep learning have made great progress, there are still some potential and unsolved problems. We summarized eight aspects, as mentioned above. The development of deep learning has entered its challenging period.

ACKNOWLEDGMENTS

This work was supported by the National Natural Science Foundation of China (Nos. 61876220, 61876221, 61976164, 61836009, U1701267, and 61871310), the Project supported the Foundation for Innovative Research Groups of the National Natural Science Foundation of China (No. 61621005), the Major Research Plan of the National Natural Science Foundation of China (Nos. 91438201 and 91438103), the Program for Cheung Kong Scholars and Innovative Research Team in University (No. IRT_15R53), the Fund for Foreign Scholars in University Research and Teaching Programs (the 111 Project) (No. B07048), the Science Foundation of Xidian University (Nos. 10251180018 and 10251180019), the National Science Basic Research Plan in Shaanxi Province of China (Nos. 2019JQ-657 and 2020JM-194), and the Key Special Project of China High Resolution Earth Observation System-Young Scholar Innovation Fund. Jun Fan was supported by the Natural Science Foundation of Hebei Province (No. A2019202135).

REFERENCES

- [1] C. Peng, W.-A. Lin, H. Liao, R. Chellappa, and S. K. Zhou, "Saint: Spatially aware interpolation network for medical slice synthesis," in *Proc. IEEE Conf. Comput. Vis. Pattern Recognit.*, 2020, pp. 7750–7759.
- [2] C. Ma, Z. Jiang, Y. Rao, J. Lu, and J. Zhou, "Deep face super-resolution with iterative collaboration between attentive recovery and landmark estimation," in *Proc. IEEE Conf. Comput. Vis. Pattern Recognit.*, 2020, pp. 5569–5578.
- [3] R. Dian, L. Fang, and S. Li, "Hyperspectral image super-resolution via non-local sparse tensor factorization," in *Proc. IEEE Conf. Comput. Vis. Pattern Recognit.*, 2017, pp. 3862–3871.
- [4] V. Fakour-Sevom, E. Guldogan, and J.-K. Kämäräinen, "360 panorama super-resolution using deep convolutional networks," in *Int. Conf. on Computer Vision Theory and Applications (VISAPP)*, vol. 1, 2018.
- [5] H. Liu, Z. Ruan, C. Fang, P. Zhao, F. Shang, Y. Liu, and L. Wang, "A single frame and multi-frame joint network for 360-degree panorama video super-resolution," *arXiv preprint arXiv:2008.10320*, 2020.
- [6] Y. Wang, R. Fevig, and R. R. Schultz, "Super-resolution mosaicking of uav surveillance video," in *Proc. IEEE Int. Conf. Image Process.*, 2008, pp. 345–348.

- [7] S. Y. Kim, J. Oh, and M. Kim, "Deep sr-itm: Joint learning of super-resolution and inverse tone-mapping for 4k uhd hdr applications," in *Proc. IEEE Conf. Comput. Vis. Pattern Recognit.*, 2019, pp. 3116–3125.
- [8] R. R. Schultz and R. L. Stevenson, "Extraction of high-resolution frames from video sequences," *IEEE Trans. Image Process.*, vol. 5, no. 6, pp. 996–1011, 1996.
- [9] M. Protter, M. Elad, H. Takeda, and P. Milanfar, "Generalizing the nonlocal-means to super-resolution reconstruction," *IEEE Trans. Image Process.*, vol. 18, no. 1, pp. 36–51, 2009.
- [10] H. Takeda, P. Milanfar, M. Protter, and M. Elad, "Super-resolution without explicit subpixel motion estimation," *IEEE Trans. Image Process.*, vol. 18, no. 9, pp. 1958–1975, 2009.
- [11] C. Liu and D. Sun, "On Bayesian adaptive video super resolution," *IEEE Trans. Pattern Anal. Mach. Intell.*, vol. 36, no. 2, pp. 346–360, 2014.
- [12] Z. Ma, R. Liao, X. Tao, L. Xu, J. Jia, and E. Wu, "Handling motion blur in multi-frame super-resolution," in *Proc. IEEE Conf. Comput. Vis. Pattern Recognit.*, 2015, pp. 5224–5232.
- [13] Z. Wang, J. Chen, and S. C. Hoi, "Deep learning for image super-resolution: A survey," *IEEE Trans. Pattern Anal. Mach. Intell.*, 2020.
- [14] A. Singh and J. Singh, "Survey on single image based super-resolution-implementation challenges and solutions," *Multimed. Tools Appl.*, vol. 79, no. 3, pp. 1641–1672, 2020.
- [15] W. Yang, X. Zhang, Y. Tian, W. Wang, J.-H. Xue, and Q. Liao, "Deep learning for single image super-resolution: A brief review," *IEEE Trans. Multimedia*, vol. 21, no. 12, pp. 3106–3121, 2019.
- [16] M. V. Daithankar and S. D. Ruikar, "Video super resolution: A review," in *ICDSMLA 2019*, 2020, pp. 488–495.
- [17] S. Farsiu, M. D. Robinson, M. Elad, and P. Milanfar, "Fast and robust multiframe super resolution," *IEEE Trans. Image Process.*, vol. 13, no. 10, pp. 1327–1344, 2004.
- [18] J. Pan, S. Cheng, J. Zhang, and J. Tang, "Deep blind video super-resolution." [Online]. Available: <http://arxiv.org/abs/2003.04716>
- [19] R. Liao, X. Tao, R. Li, Z. Ma, and J. Jia, "Video super-resolution via deep draft-ensemble learning," in *Proc IEEE Int. Conf. Comput. Vis.*, 2015, pp. 531–539.
- [20] A. Kappeler, S. Yoo, Q. Dai, and A. K. Katsaggelos, "Video super-resolution with convolutional neural networks," *IEEE Trans. Comput. Imaging*, vol. 2, no. 2, pp. 109–122, June 2016.
- [21] J. Caballero, C. Ledig, A. Aitken, A. Acosta, J. Totz, Z. Wang, and W. Shi, "Real-time video super-resolution with spatio-temporal networks and motion compensation," in *Proc. IEEE Conf. Comput. Vis. Pattern Recognit.*, 2017, pp. 2848–2857.
- [22] X. Tao, H. Gao, R. Liao, J. Wang, and J. Jia, "Detail-revealing deep video super-resolution," in *Proc IEEE Int. Conf. Comput. Vis.*, 2017, pp. 4482–4490.
- [23] D. Liu, Z. Wang, Y. Fan, X. Liu, Z. Wang, S. Chang, and T. Huang, "Robust video super-resolution with learned temporal dynamics," in *Proc IEEE Int. Conf. Comput. Vis.*, 2017, pp. 2526–2534.
- [24] M. S. M. Sajjadi, R. Vemulapalli, and M. Brown, "Frame-recurrent video super-resolution," in *Proc. IEEE Conf. Comput. Vis. Pattern Recognit.*, 2018, pp. 6626–6634.
- [25] T. H. Kim, M. S. M. Sajjadi, M. Hirsch, and B. Schölkopf, "Spatio-temporal transformer network for video restoration," in *Comput. Vis. - ECCV*, 2018, pp. 111–127.
- [26] L. Wang, Y. Guo, Z. Lin, X. Deng, and W. An, "Learning for video super-resolution through HR optical flow estimation," in *Proc. Asian Conf. Comput. Vis.*, 2019, pp. 514–529.
- [27] M. Chu, Y. Xie, J. Mayer, L. Leal-Taixé, and N. Thuerey, "Learning Temporal Coherence via Self-Supervision for GAN-based Video Generation," *arXiv e-prints*, 2018.
- [28] T. Xue, B. Chen, J. Wu, D. Wei, and W. T. Freeman, "Video enhancement with task-oriented flow," *Int. J. Comput. Vis.*, vol. 127, no. 8, pp. 1106–1125, Aug 2019.
- [29] Z. Wang, P. Yi, K. Jiang, J. Jiang, Z. Han, T. Lu, and J. Ma, "Multi-memory convolutional neural network for video super-resolution," *IEEE Trans. Image Process.*, vol. 28, no. 5, pp. 2530–2544, May 2019.
- [30] M. Haris, G. Shakhnarovich, and N. Ukita, "Recurrent back-projection network for video super-resolution," in *Proc. IEEE Conf. Comput. Vis. Pattern Recognit.*, 2019, pp. 3892–3901.
- [31] W. Bao, W. Lai, X. Zhang, Z. Gao, and M. Yang, "MEMC-Net: Motion estimation and motion compensation driven neural network for video interpolation and enhancement," *IEEE Trans. Pattern Anal. Mach. Intell.*, 2019.
- [32] D. Li, Y. Liu, and Z. Wang, "Video super-resolution using non-simultaneous fully recurrent convolutional network," *IEEE Trans. Image Process.*, vol. 28, no. 3, pp. 1342–1355, March 2019.
- [33] B. Bare, B. Yan, C. Ma, and K. Li, "Real-time video super-resolution via motion convolution kernel estimation," *Neurocomputing*, vol. 367, pp. 236–245, 2019.
- [34] R. Kalarot and F. Porikli, "MultiBoot VSR: Multi-stage multi-reference bootstrapping for video super-resolution," in *Proc. IEEE Conf. Comput. Vis. Pattern Recognit. Workshops*, 2019, pp. 2060–2069.
- [35] J. Xin, N. Wang, J. Li, X. Gao, and Z. Li, "Video face super-resolution with motion-adaptive feedback cell," in *Proc. AAAI Conf. Artif. Intell.*, 2020, pp. 12 468–12 475.
- [36] M. Haris, G. Shakhnarovich, and N. Ukita, "Space-

- time-aware multi-resolution video enhancement," in *Proc. IEEE/CVF Conf. Comput. Vis. Pattern Recognit.*, 2020, pp. 2859–2868.
- [37] X. Wang, K. C. K. Chan, K. Yu, C. Dong, and C. C. Loy, "EDVR: Video restoration with enhanced deformable convolutional networks," in *Proc. IEEE Conf. Comput. Vis. Pattern Recognit. Workshops*, 2019, pp. 1954–1963.
- [38] H. Wang, D. Su, C. Liu, L. Jin, X. Sun, and X. Peng, "Deformable non-local network for video super-resolution," *IEEE Access*, vol. 7, pp. 177 734–177 744, 2019.
- [39] Y. Tian, Y. Zhang, Y. Fu, and C. Xu, "TDAN: Temporally-deformable alignment network for video super-resolution," in *Proc. IEEE Conf. Comput. Vis. Pattern Recognit.*, 2020, pp. 3360–3369.
- [40] X. Ying, L. Wang, Y. Wang, W. Sheng, W. An, and Y. Guo, "Deformable 3d convolution for video super-resolution," *arXiv preprint arXiv:2004.02803*, 2020.
- [41] J. Chen, X. Tan, C. Shan, S. Liu, and Z. Chen, "Vesr-net: The winning solution to youku video enhancement and super-resolution challenge," *arXiv preprint arXiv:2003.02115*, 2020.
- [42] A. Lucas, S. LApez-Tapia, R. Molina, and A. K. Katsaggelos, "Generative adversarial networks and perceptual losses for video super-resolution," *IEEE Trans. Image Process.*, vol. 28, no. 7, pp. 3312–3327, July 2019.
- [43] B. Yan, C. Lin, and W. Tan, "Frame and feature-context video super-resolution," in *Proc. AAAI Conf. Artif. Intell.*, 2019, pp. 5597–5604.
- [44] Y. Jo, S. W. Oh, J. Kang, and S. J. Kim, "Deep video super-resolution network using dynamic up-sampling filters without explicit motion compensation," in *Proc. IEEE Conf. Comput. Vis. Pattern Recognit.*, 2018, pp. 3224–3232.
- [45] S. Li, F. He, B. Du, L. Zhang, Y. Xu, and D. Tao, "Fast spatio-temporal residual network for video super-resolution," in *Proc. IEEE Conf. Comput. Vis. Pattern Recognit.*, 2019, pp. 10 522–10 531.
- [46] S. Y. Kim, J. Lim, T. Na, and M. Kim, "Video super-resolution based on 3d-cnns with consideration of scene change," in *Proc. IEEE Int. Conf. Image Process.*, 2019, pp. 2831–2835.
- [47] Y. Huang, W. Wang, and L. Wang, "Bidirectional recurrent convolutional networks for multi-frame super-resolution," in *Advances in Neural Information Processing Systems*, 2015, pp. 235–243.
- [48] Y. Huang, W. Wang, and L. Wang, "Video super-resolution via bidirectional recurrent convolutional networks," *IEEE Trans. Pattern Anal. Mach. Intell.*, vol. 40, no. 4, pp. 1015–1028, April 2018.
- [49] J. Guo and H. Chao, "Building an end-to-end spatial-temporal convolutional network for video super-resolution," in *Proc. AAAI Conf. Artif. Intell.*, 2017, pp. 4053–4060.
- [50] X. Zhu, Z. Li, X. Zhang, C. Li, Y. Liu, and Z. Xue, "Residual invertible spatio-temporal network for video super-resolution," in *Proc. AAAI Conf. Artif. Intell.*, 2019, pp. 5981–5988.
- [51] P. Yi, Z. Wang, K. Jiang, J. Jiang, and J. Ma, "Progressive fusion video super-resolution network via exploiting non-local spatio-temporal correlations," in *Proc IEEE Int. Conf. Comput. Vis.*, 2019, pp. 3106–3115.
- [52] W. Li, X. Tao, T. Guo, L. Qi, J. Lu, and J. Jia, "Mucan: Multi-correspondence aggregation network for video super-resolution," *arXiv preprint arXiv:2007.11803*, 2020.
- [53] C. Dong, C. C. Loy, K. He, and X. Tang, "Learning a deep convolutional network for image super-resolution," in *Eur. Conf. Comput. Vis.*, 2014, pp. 184–199.
- [54] C. Dong, C. C. Loy, and X. Tang, "Accelerating the super-resolution convolutional neural network," in *Eur. Conf. Comput. Vis.*, 2016, pp. 391–407.
- [55] J. Kim, J. K. Lee, and K. M. Lee, "Accurate image super-resolution using very deep convolutional networks," in *Proc. IEEE Conf. Comput. Vis. Pattern Recognit.*, 2016, pp. 1646–1654.
- [56] W. Shi, J. Caballero, F. Huszr, J. Totz, A. P. Aitken, R. Bishop, D. Rueckert, and Z. Wang, "Real-time single image and video super-resolution using an efficient sub-pixel convolutional neural network," in *Proc. IEEE Conf. Comput. Vis. Pattern Recognit.*, 2016, pp. 1874–1883.
- [57] Y. Zhang, Y. Tian, Y. Kong, B. Zhong, and Y. Fu, "Residual dense network for image super-resolution," in *Proc. IEEE/CVF Conf. Comput. Vis. Pattern Recognit.*, 2018, pp. 2472–2481.
- [58] Y. Zhang, K. Li, K. Li, L. Wang, B. Zhong, and Y. Fu, "Image super-resolution using very deep residual channel attention networks," in *Comput. Vis. - ECCV*, 2018, pp. 294–310.
- [59] A. Shocher, N. Cohen, and M. Irani, "Zero-shot super-resolution using deep internal learning," in *Proc. IEEE/CVF Conf. Comput. Vis. Pattern Recognit.*, 2018, pp. 3118–3126.
- [60] C. Ledig, L. Theis, F. Huszr, J. Caballero, A. Cunningham, A. Acosta, A. Aitken, A. Tejani, J. Totz, Z. Wang, and W. Shi, "Photo-realistic single image super-resolution using a generative adversarial network," in *Proc. IEEE Conf. Comput. Vis. Pattern Recognit.*, 2017, pp. 105–114.
- [61] A. Dosovitskiy, P. Fischer, E. Ilg, P. Husser, C. Hazirbas, V. Golkov, P. v. d. Smagt, D. Cremers, and T. Brox, "FlowNet: Learning optical flow with convolutional networks," in *Proc IEEE Int. Conf. Comput. Vis.*, 2015, pp. 2758–2766.
- [62] B. D. Lucas and T. Kanade, "An iterative image registration technique with an application to stereo vision," in *Proc. Int. Joint Conf. Artif. Intell.*, 1981, pp. 674–679.
- [63] M. Drulea and S. Nedeveschi, "Total variation regularization of local-global optical flow," in *2011 14th*

- International IEEE Conf Intell Transport Syst (ITSC)*, 2011, pp. 318–323.
- [64] E. Ilg, N. Mayer, T. Saikia, M. Keuper, A. Dosovitskiy, and T. Brox, “FlowNet 2.0: Evolution of optical flow estimation with deep networks,” in *Proc. IEEE Conf. Comput. Vis. Pattern Recognit.*, 2017, pp. 1647–1655.
- [65] A. Ranjan and M. J. Black, “Optical flow estimation using a spatial pyramid network,” in *Proc. IEEE Conf. Comput. Vis. Pattern Recognit.*, 2017, pp. 2720–2729.
- [66] M. Jaderberg, K. Simonyan, A. Zisserman, and k. kavukcuoglu, “Spatial transformer networks,” in *Adv. neural inf. proces. syst.* 28, 2015, pp. 2017–2025.
- [67] T. Brox, A. Bruhn, N. Papenberger, and J. Weickert, “High accuracy optical flow estimation based on a theory for warping,” in *Comput. Vis. - ECCV*, T. Pajdla and J. Matas, Eds., 2004, pp. 25–36.
- [68] C. Liu *et al.*, “Beyond pixels: exploring new representations and applications for motion analysis,” Ph.D. dissertation, Massachusetts Institute of Technology, 2009.
- [69] L. Xu, J. Jia, and Y. Matsushita, “Motion detail preserving optical flow estimation,” *IEEE Trans. Pattern Anal. Mach. Intell.*, vol. 34, no. 9, pp. 1744–1757, Sep. 2012.
- [70] X. Shi, Z. Chen, H. Wang, D.-Y. Yeung, W.-k. Wong, and W.-c. Woo, “Convolutional LSTM network: A machine learning approach for precipitation now-casting,” in *Adv. neural inf. proces. syst.* 28, 2015, pp. 802–810.
- [71] O. Ronneberger, P. Fischer, and T. Brox, “U-net: Convolutional networks for biomedical image segmentation,” in *Medical Image Computing and Computer-Assisted Intervention – MICCAI*, 2015, pp. 234–241.
- [72] G. Huang, Z. Liu, L. Van Der Maaten, and K. Q. Weinberger, “Densely connected convolutional networks,” in *Proc. IEEE Conf. Comput. Vis. Pattern Recognit.*, 2017, pp. 2261–2269.
- [73] M. Irani and S. Peleg, “Improving resolution by image registration,” *CVGIP Graphical Models Image Process*, vol. 53, no. 3, pp. 231 – 239, 1991.
- [74] “Motion analysis for image enhancement: Resolution, occlusion, and transparency,” *J. Vis. Commun. Image Represent.*, vol. 4, no. 4, pp. 324 – 335, 1993.
- [75] M. Haris, G. Shakhnarovich, and N. Ukita, “Deep back-projection networks for super-resolution,” in *Proc. IEEE Conf. Comput. Vis. Pattern Recognit.*, 2018, pp. 1664–1673.
- [76] B. Lim, S. Son, H. Kim, S. Nah, and K. M. Lee, “Enhanced deep residual networks for single image super-resolution,” in *Proc. IEEE Conf. Comput. Vis. Pattern Recognit. Workshops*, 2017, pp. 1132–1140.
- [77] K. He, X. Zhang, S. Ren, and J. Sun, “Deep residual learning for image recognition,” in *Proc. IEEE Conf. Comput. Vis. Pattern Recognit.*, 2016, pp. 770–778.
- [78] K. Li, B. Bare, B. Yan, B. Feng, and C. Yao, “Face hallucination based on key parts enhancement,” in *Proc. IEEE Int. Conf. Acoust. Speech Signal. Process.*, 2018, pp. 1378–1382.
- [79] J. Dai, H. Qi, Y. Xiong, Y. Li, G. Zhang, H. Hu, and Y. Wei, “Deformable convolutional networks,” in *Proc IEEE Int. Conf. Comput. Vis.*, 2017, pp. 764–773.
- [80] X. Zhu, H. Hu, S. Lin, and J. Dai, “Deformable ConvNets V2: More deformable, better results,” in *Proc. IEEE Conf. Comput. Vis. Pattern Recognit.*, 2019, pp. 9300–9308.
- [81] S. Nah, S. Baik, S. Hong, G. Moon, S. Son, R. Timofte, and K. M. Lee, “NTIRE 2019 challenge on video deblurring and super-resolution: Dataset and study,” in *Proc. IEEE Conf. Comput. Vis. Pattern Recognit. Workshops*, 2019, pp. 1996–2005.
- [82] S. Nah, R. Timofte, S. Gu, S. Baik, S. Hong *et al.*, “NTIRE 2019 challenge on video super-resolution: Methods and results,” in *Proc. IEEE Conf. Comput. Vis. Pattern Recognit. Workshops*, 2019, pp. 1985–1995.
- [83] D. Sun, X. Yang, M. Liu, and J. Kautz, “PWC-Net: CNNs for optical flow using pyramid, warping, and cost volume,” in *Proc. IEEE Conf. Comput. Vis. Pattern Recognit.*, 2018, pp. 8934–8943.
- [84] T. Hui, X. Tang, and C. C. Loy, “LiteFlowNet: A lightweight convolutional neural network for optical flow estimation,” in *Proc. IEEE Conf. Comput. Vis. Pattern Recognit.*, 2018, pp. 8981–8989.
- [85] —, “A lightweight optical flow cnn - revisiting data fidelity and regularization,” *IEEE Trans. Pattern Anal. Mach. Intell.*, 2020.
- [86] X. Wang, R. Girshick, A. Gupta, and K. He, “Non-local neural networks,” in *Proc. IEEE Conf. Comput. Vis. Pattern Recognit.*, 2018, pp. 7794–7803.
- [87] Z. Hui, J. Li, X. Gao, and X. Wang, “Progressive perception-oriented network for single image super-resolution,” *CoRR*, vol. abs/1907.10399, 2019. [Online]. Available: <http://arxiv.org/abs/1907.10399>
- [88] X. Xiang, Y. Tian, Y. Zhang, Y. Fu, J. P. Allebach, and C. Xu, “Zooming slow-mo: Fast and accurate one-stage space-time video super-resolution,” in *Proc. IEEE/CVF Conf. Comput. Vis. Pattern Recognit.*, 2020, pp. 3370–3379.
- [89] D. Tran, L. Bourdev, R. Fergus, L. Torresani, and M. Paluri, “Learning spatiotemporal features with 3d convolutional networks,” in *Proc IEEE Int. Conf. Comput. Vis.*, 2015, pp. 4489–4497.
- [90] S. Ji, W. Xu, M. Yang, and K. Yu, “3D convolutional neural networks for human action recognition,” *IEEE Trans. Pattern Anal. Mach. Intell.*, vol. 35, no. 1, pp. 221–231, Jan 2013.
- [91] X. Jia, B. De Brabandere, T. Tuytelaars, and L. V. Gool, “Dynamic filter networks,” in *Adv. neural inf. proces. syst.* 29, 2016, pp. 667–675.
- [92] S. Hochreiter and J. Schmidhuber, “Long short-

- term memory," *Neural Comput.*, vol. 9, no. 8, pp. 1735–1780, 1997.
- [93] J.-H. Jacobsen, A. W. Smeulders, and E. Oyallon, "i-RevNet: Deep invertible networks," in *Proc. Int. Conf. Learn. Represent.*, 2018.
 - [94] F. Dario, Z. Huang, S. Gu, T. Radu *et al.*, "Aim 2020 challenge on video extreme super-resolution: Methods and results," *arXiv preprint arXiv:2007.11803*, 2020.
 - [95] K. Seshadrinathan and A. C. Bovik, "Motion tuned spatio-temporal quality assessment of natural videos," *IEEE Trans. Image Process.*, vol. 19, no. 2, pp. 335–350, 2010.
 - [96] R. Zhang, P. Isola, A. A. Efros, E. Shechtman, and O. Wang, "The unreasonable effectiveness of deep features as a perceptual metric," in *Proc. IEEE Conf. Comput. Vis. Pattern Recognit.*, 2018, pp. 586–595.
 - [97] D. P. Kingma and J. Ba, "Adam: A method for stochastic optimization," in *Proc. Int. Conf. Learn. Represent.*, 2015.
 - [98] X. Glorot and Y. Bengio, "Understanding the difficulty of training deep feedforward neural networks," in *Proceedings of the Thirteenth International Conference on Artificial Intelligence and Statistics*, 2010, pp. 249–256.
 - [99] J. Pont-Tuset, F. Perazzi, S. Caelles, P. Arbeláez, A. Sorkine-Hornung, and L. Van Gool, "The 2017 DAVIS Challenge on Video Object Segmentation," *arXiv e-prints*, p. arXiv:1704.00675, Apr 2017.
 - [100] K. Simonyan and A. Zisserman, "Very deep convolutional networks for large-scale image recognition," in *Proc. Int. Conf. Learn. Represent.*, 2015.
 - [101] O. Shahar, A. Faktor, and M. Irani, "Space-time super-resolution from a single video," in *Proc. IEEE Conf. Comput. Vis. Pattern Recognit.*, 2011, pp. 3353–3360.
 - [102] J. Kim, J. K. Lee, and K. M. Lee, "Deeply-recursive convolutional network for image super-resolution," in *Proc. IEEE Conf. Comput. Vis. Pattern Recognit.*, 2016, pp. 1637–1645.
 - [103] Y. Tai, J. Yang, and X. Liu, "Image super-resolution via deep recursive residual network," in *Proc. IEEE Conf. Comput. Vis. Pattern Recognit.*, 2017, pp. 2790–2798.

Supplementary Materials for “Video Super Resolution Based on Deep Learning: A Comprehensive Survey”

In this supplementary material, we first present some background of video super-resolution tasks including the video quality metrics for SR results. Moreover, we provide the training details of all the representative VSR methods including the training process, loss function, and datasets. Finally, we report more experimental results for the cases of scale factors 2 and 3.

IX. BACKGROUND

Like images, video quality is mainly evaluated by calculating PSNR and SSIM, which measure the difference of pixels and similarity of structures between two images as follows. PSNR of one SR frame is defined as:

$$\text{PSNR} = 10 \log_{10} \left(\frac{L^2}{\text{MSE}} \right) \quad (7)$$

where L represents the maximum range of color value, which is usually 255, and the mean squared error (MSE) is defined as:

$$\text{MSE} = \frac{1}{N} \sum_{i=1}^N (\hat{I}(i) - \tilde{I}(i))^2 \quad (8)$$

where N denotes the total number of pixels in an image or a frame. Here \hat{I} and \tilde{I} denote the ground truth HR frame and the SR recovered frame, respectively. A higher value of PSNR generally means superior quality. In addition, SSIM is defined as:

$$\text{SSIM}(\hat{I}, \tilde{I}) = \frac{2u_{\hat{I}}u_{\tilde{I}} + k_1}{u_{\hat{I}}^2 + u_{\tilde{I}}^2 + k_1} \cdot \frac{2\sigma_{\hat{I}\tilde{I}} + k_2}{\sigma_{\hat{I}}^2 + \sigma_{\tilde{I}}^2 + k_2} \quad (9)$$

where $u_{\hat{I}}$ and $u_{\tilde{I}}$ represent the mean values of the images \hat{I} and \tilde{I} , respectively. k_1 and k_2 are constants, which are used to stabilize the calculation and are usually set to 0.01 and 0.03, respectively. $\sigma_{\hat{I}}$ and $\sigma_{\tilde{I}}$ denote the standard deviations, and $\sigma_{\hat{I}\tilde{I}}$ denotes the covariance. They are defined as:

$$u_{\hat{I}} = \frac{1}{N} \sum_{i=1}^N \hat{I}(i), \quad (10)$$

$$\sigma_{\hat{I}} = \left[\frac{1}{N-1} \sum_{i=1}^N (\hat{I}(i) - u_{\hat{I}})^2 \right]^{\frac{1}{2}}, \quad (11)$$

$$\sigma_{\hat{I}\tilde{I}} = \frac{1}{N-1} \sum_{i=1}^N (\hat{I}(i) - u_{\hat{I}})(\tilde{I}(i) - u_{\tilde{I}}). \quad (12)$$

Moreover, considering the characteristics of video sequences, several measurements have been proposed and used for the evaluation of recovered video quality, including MOVIE [95, 21], Learned Perceptual Image Patch Similarity (LPIPS) [96] and the two measurements: tOF and tLP, which were proposed in [27].

X. METHODS WITH ALIGNMENT

The methods with alignment make neighboring frames align with the target frame by using extracted motion information through networks before subsequent reconstruction. And the methods mainly use motion compensation or deformable convolution, which are two common techniques for aligning frames. Next we will introduce state-of-art methods based on each of the techniques in details.

A. Motion Estimation and Compensation Methods

Video super-resolution algorithms based on optical flow methods usually need to perform motion estimation and motion compensation before subsequent operations, where the estimation process is implemented by optical flow algorithms and the compensation process can be implemented by multiple ways, such as bilinear interpolation and spatial transformer network (STN) [66]. Motion estimation is used to extract motion information between frames, while motion compensation is used to perform image transformation between images in terms of motion information to make neighboring frames spatially align with the target frame.

1) *Deep-DE*: Deep-DE uses the ℓ_1 -norm loss with a total variation regularization as its loss function.

2) *VSRnet*: VSRnet adopts the Myanmar²⁰ videos as training dataset, whose resolution is $3,840 \times 2,160$. In the experiment, the ground truth videos are collected by down-sampling original videos to the resolution of 960×540 . LR videos are obtained by performing a bicubic interpolation. More specially, the input frames are upsampled before feeding into the network and the number of input frames is 5. Then the frames are converted to YCbCr color space, where the Y channel is used for training the network and performance assessment. The testing set is the Vid4²¹ dataset, which consists of four common videos including city, calendar, walk and foliage. The numbers of frames for the four videos are 34, 41, 47, and 49, respectively, and their resolutions are 704×576 , 720×576 , 720×480 and 720×480 , respectively. The training strategy of VSRnet is that the pre-trained SRCNN is used to initialize the network weights in order to reduce the dependence on large-scale video datasets. Then VSRnet is trained with small-scale video datasets. The loss function of VSRnet is the MSE loss.

3) *VESPCN*: VESPCN uses the videos collected from the CDVL database²² as the training dataset, which includes 115 videos with size $1,920 \times 1,080$, and Vid4 is used as testing dataset. The LR videos are obtained by downsampling from the HR videos. The number of input frames is set to 3. The loss function consists of both MSE and motion compensation (MC) loss. The MC loss denotes the difference between the warped frame and the target frame. The network applies the Adam

²⁰<https://www.harmonicinc.com/>

²¹<https://twitter.box.com/v/vespcn-vid4>

²²<http://www.cdvl.org/>

[97] optimizer for training. The batch size is 16, and the learning rate is set to 10^{-4} .

4) *DRVSR*: The training of DRVSR is divided into three stages. First of all, the motion estimation module is trained with its motion compensation loss. Then the parameters of the trained motion estimation module are fixed, and the fusion module is trained based on the MSE loss. Finally, the entire network is fine-tuned using the total loss of MSE and motion compensation loss. Moreover, in order to make training process stable, DRVSR adopts the gradient clip strategy to constrain the weight of ConvLSTM. Adam is used as the optimizer and the network weights are initialized by the Xavier [98], which is an efficient initialization method.

5) *RVSR*: RVSR adopts the videos from the LIVE video quality assessment database, the MCL-V database, and the TUM 1080p dataset as the training set, and meanwhile employs data augmentation techniques. The Vid4, penguin (pg) [19], temple (tp) [19] and Ultra Video Group Database (UVGD)²³ are adopted as testing set. The number of input frames is 5, and the patch size is set to 30×30 . RVSR combines the loss of both the spatial alignment module and spatio-temporal adaptive module as the final loss function, in which the loss of the spatio-temporal adaptive module is the difference between the GT and the network output. And the loss of the spatial alignment module is the difference between the GT transformation parameters and transformation parameters estimated by the localization net. And the GT transformation parameters are obtained by the rectified optical flow alignment.

6) *FRVSR*: In FRVSR, the optical flow network consists of 14 convolutional layers, 3 pooling layers and 3 bilinear upsampling layers. Each convolutional layer is followed by a LeakyReLU activation function, except for the last convolutional layer. The super-resolution network consists of 2 convolutional layers, 2 deconvolutional layers with downsampling factor 2, and 10 residual blocks. And each residual block consists of 2 convolutional layers and a ReLU activation function. FRVSR adopts the combination of MSE and motion compensation loss as its loss function, Adam as the optimizer of the network and Vid4 as testing set.

7) *STTN*: STTN adopts the combination of MSE and motion compensation loss as its loss function.

8) *SOFVSR*: SOFVSR adopts 145 videos from the CDVL database as training set, 7 videos from the Ultra Video Group database²⁴ as validation set, and Vid4 and 10 videos from the DAVIS dataset [99] as testing set. SOFVSR converts the RGB color space into the YCbCr color space and only uses the Y channel to train the network. The number of input frames is 3. Patch size is set to 32×32 , and data augmentation techniques are also used. The loss function includes the MSE and motion compensation loss, where the motion compensation loss

includes three parts corresponding to three stages of OFNet, and each stage computes a motion compensation loss by using current optical flow. Adam is used as the optimizer for training the network. The initial learning rate is set to 10^{-4} and reduces by half after every 50,000 iterations.

9) *TecoGAN*: The loss function of TecoGAN consists of 6 parts including MSE, adversarial loss, feature space loss from discriminator, perceptual loss, “ping-pong” loss and motion compensation loss. Adam is used as the optimizer, Vid4 and Tear of Steel (ToS) are used as testing set. Similar to other GAN-based methods, training makes the discriminator unable to distinguish whether the HR image generated from the generator is a GT frame or synthetic super-resolution frame. Although these methods can yield HR videos with better perception quality, the PSNR value is usually relatively low, which may highlight the flaw of PSNR in assessing image and video quality.

10) *TOFlow*: TOFlow presents a new dataset, called Vimeo-90K, for training and testing video sequences. Vimeo-90K consists of 4,278 videos including 89,800 different independent scenes. TOFlow adopts the L1-norm as its loss function. For video super-resolution, TOFlow takes 7 upsampled consecutive frames as input. Besides Vimeo-90K, TOFlow also uses Vid4 as its testing dataset.

11) *MMCNN*: For motion estimation and motion compensation, MMCNN adopts MCT in VESPCN [21]. The number of input frames is set to 5. The loss function consists of both the MSE and motion compensation loss. The *Myanmar*¹ testing set, YUV21²⁵, and Vid4 are used as testing datasets.

12) *RBP*: In RBP, DBPN [75] is adopted as the single image super-resolution network, and ResNet [77] with deconvolution is used as the multi-image super-resolution network. RBP uses the Vimeo-90K [28] dataset as training set and testing set, and meanwhile uses data augmentation techniques. Batch size and patch size are set to 8 and 64×64 , respectively. The ℓ_1 -norm loss and Adam are used as the training loss function and optimizer, respectively. The initial learning rate is set to 10^{-4} , and it reduces to one tenth of the initial learning rate when runs half of the total iterations.

13) *MEMC-Net*: In MEMC-Net, the architecture of the super-resolution module is similar to that of EDSR [76]. In addition, in order to deal with the occlusion problem, it adopts a pre-trained ResNet18 [77] to extract the feature of input frames. Moreover, it feeds the output of the first convolutional layer of ResNet18 as the context information into the adaptive warping layer to perform the same warp operation. MEMC-Net adopts Vimeo-90K as training set and testing set, the Charbonnier (Cb) function as the loss function, and Adam [97] as the optimizer for the network.

²³<http://ultravideo.cs.tut.fi/>

²⁴ultravideo.cs.tut.fi

²⁵<http://www.codersvoice.com/a/webbase/video/08/152014/130.html>

The Cb function is defined as:

$$\mathcal{L} = \frac{1}{N} \sum_{i=1}^N \sqrt{\|\hat{I}_t^i - I_t^i\|_2^2 + \epsilon^2} \quad (13)$$

where $\|x\|_2$ denotes the ℓ_2 -norm ($\|x\|_2 = \sqrt{\sum_i x_i^2}$), N equals to the size of batch, and ϵ is set to 0.001.

14) *RRCN*: The proposed RRCN consists of 15 convolutional layers. Except the last layer, the forward convolution in other layers uses the 3×3 convolutional kernel and 32 feature maps. In the last layer, though it uses the 3×3 convolutional kernel, the number of feature maps depends on the final output format. The recurrent convolution is with 1×1 kernel and 32 feature maps. Moreover, RRCN uses the Myanmar video as training set, and Myanmar (except for training data), Vid4, and YUV21 as testing set. MSE is used as the loss function, and RMSProp is used as the optimization method. The number of input frames is 5, and the patch size is 81×81 . The up-sampled and compensated LR frames are used as the inputs for RRCN.

15) *RTVSR*: RTVSR first adopts the motion convolutional kernel network for the convolutional kernel estimation of the target frame and neighboring frame, and produces a pair of 1D convolutional kernels that represent the horizontal and vertical directions, respectively. Then the estimated convolutional kernels are used to warp the neighboring frame. After that the warped frame and target frame are fed into the subsequent SR module to obtain the super-resolution result of the target frame. RTVSR designs an important component called gated enhance units (GEUs) to learn useful features, which is an improved variant based on [78]. In GEUs, the output of residual blocks is not an element-wise addition between the input and output, but is a sum of the input and output with learned weights.

RTVSR uses 261 videos with resolution of $3,840 \times 2,160$ from harmonicinc.com as the training set and adopts data augmentation to enlarge the training set. The GT videos are obtained by downsampling the original videos to the resolution of 960×540 . Vid4 is used as the testing set. RTVSR utilizes Adam as the optimizer and MSE as loss function. Patch size and batch size are set to 96×96 and 64, respectively.

16) *MultiBoot VSR*: The LR frames are input to the FlowNet 2.0 [64] to compute optical flow and perform the motion compensation operation. Then the processed frames are fed into the first-stage network to attain the super-resolution result of the target frame. In the second stage of MultiBoot VSR, the output from the previous stage is downsampled, concatenated with the initial LR frame, and then input to the network to obtain the final super-resolution result for the target frame.

MultiBoot VSR adopts REDS [81, 82] as training set and testing set. Moreover, it also employs commonly used data augmentation techniques. The Huber loss

function \mathcal{H} is used for training, and is defined as:

$$\mathcal{H}(I_t - \tilde{I}_t) = \begin{cases} \frac{1}{2} \|I_t - \tilde{I}_t\|_2^2, & \|I_t - \tilde{I}_t\|_1 \leq \delta, \\ \delta \|I_t - \tilde{I}_t\|_1 - \frac{1}{2} \delta^2, & \text{otherwise} \end{cases} \quad (14)$$

where $\|x\|_1$ denotes the ℓ_1 -norm ($\|x\|_1 = \sum_i |x_i|$), I_t and \tilde{I}_t denote the HR image and the estimated HR image at time t . Note that $\delta = 1$, which is the point where the Huber loss function changes from a quadratic function to a linear one.

17) *MAFN*: For the proposed MAFC, it firstly throws away the redundant information from the cell state by a motion screen unit (MSU), which operates reduction after a convolutional layer and a sigmoid layer. The updated information is then normalized and used to infer the candidate values of motion compensation by a compensation estimation unit (CEU), which consists of two convolutional layers and a sigmoid layer. Finally, the two strategies are combined to create the final cell state, which is used as motion compensation features. It is noted that MAFC utilizes weight sharing to ensure the fairness of motion compensation between any frames.

MAFN conducts experiments on VoxCeleb dataset. It contains over 1 million utterances for 6,112 celebrities extracted from videos uploaded to YouTube, which provides the sequences of tracked faces in the form of bounding boxes. Here, 3884 video sequences of 100 people are selected for training, 10 video sequences of 5 people for verification and 697 sequences of 18 people for testing. Each sequence is computed a box enclosing the faces from all frames to crop face images from the original video. All face images are then resized to 128×128 . MAFN uses MSE as the loss function and Adam as the optimizer whose momentum parameter is set to 0.1 and the weight decay set to 2×10^{-4} . The batch size is 16, and the initial learning rate is set to 10^{-3} which is divided a half every 10 epochs.

18) *STARnet*: All the outputs from S-SR and motion modules are sent to ST-SR module to interpolate a frame in both LR and HR spaces. By the above steps, the initialization stage finally outputs processed LR feature maps of the original input frames and their interpolated frames as well as their results in HR space. The refinement stage can extract more precise spatio-temporal information for the outputs of the previous stage. In LR space, only the information of the interpolated frame are refined and preserved, while all the information are processed with the same operation in HR space. Finally, the outputs from the refinement stage are restored to corresponding frames by the reconstruction module.

STARnet employs the Vimeo-90K dataset without cropping as training set. The data is augmented by random flipping and rotation. For test, It adopts the Vimeo, UCF101 and Middlebury as test set. UCF101 is used for evaluating the performance of video interpolation. It consists of 379 triplets with resolution 256×256 . Middlebury contains 33 videos with resolution 640×480 .

STARnet evaluates interpolation error (IE) in addition to PSNR and SSIM. STARnet uses three loss functions: space loss (for super-resolution restraint), time loss (for LR interpolation result restraint) and space-time loss (for HR interpolation result restraint). The weights of the three losses are separately 1, 0.1 and 0.1. The optimizer is AdaMax with momentum 0.9, and the learning rate is initially set to 10^{-4} , which is decreased by a factor of 10 for every 30 epochs. For each fine-tuned model, another 20 epochs are used with the same learning rate and decreased by a factor of 10 for every 10 epochs.

B. Deformable Convolution Methods

1) *EDVR*: EDVR uses the realistic and dynamic scenes (REDS) dataset which is proposed in the NTIRE19 Challenge as training set. The dataset is composed of 300 video sequences with resolution of $720 \times 1,280$, and each video has 100 frames, where the training set, the validation set and the testing set include 240, 30 and 30 videos, respectively. In the experiment, because the ground truth of the testing set can not be obtained, the authors re-group the rest of the videos. They select 4 representative videos (REDS4) as testing set, and the rest of videos are used as the training set after data augmentation. In addition, EDVR adopts the Cb function as the loss function and Adam as the optimizer, and it takes five consecutive frames as inputs. Patch size and batch size are set to 64×64 and 32, respectively. The initial learning rate is set to 4×10^{-4} .

2) *DNLN*: The whole network of DNLN consists of a feature extraction module, an alignment module, a non-local attention module, one reconstruction module and one upsample module. The feature extraction module is composed of one convolutional layer and 5 residual blocks. The alignment module consists of 5 deformable convolutional layers, and the reconstruction module is made up of 16 residual in residual dense blocks (RRDB). The features of the target frame and the neighboring frame are first extracted by the feature extraction module, and then their features are fed into the alignment module to make the feature of the neighboring frame align with the feature of the target frame. The aligned features and target feature are fed into the non-local attention module to extract their correlations, and then the extracted correlations are fused by the reconstruction module. The output of the reconstruction module is added to the feature of the target frame, whose result is then up-sampled by an upsampling layer to attain the final super-resolution result for the target frame.

DNLN adopts Vimeo-90K as training set, and also uses data augmentation techniques. LR images are generated by downscaling the HR images with factor $\times 4$. Patch size is set to 50×50 . DNLN uses the ℓ_1 -norm loss as the loss function and Adam as the optimizer.

3) *TDAN*: TDAN adopts Vimeo-90K as training set, and uses the combination of the ℓ_1 -norm loss and motion compensation loss as the loss function, and Adam as the

optimizer. The initial learning rate is set to 10^{-4} . Five consecutive frames are taken as inputs. Patch size and batch size are set to 48×48 and 64, respectively.

4) *D3Dnet*: Each ResD3D block consists of a deformable 3D convolution (D3D) layer, a leakyrelu (LReLU) layer and another D3D layer. Then, a bottleneck layer is employed to fuse the compensated video sequence to a reference feature. Finally, the fused feature is processed by 6 cascaded residual blocks and the upsample module to reconstruct the SR reference frame. Each residual block consists of a traditional 3×3 convolution layer, a LReLU layer and another D3D layer.

D3Dnet employs the Vimeo-90K dataset as training set, whose LR frames are then randomly cropped to patches with size 32×32 and a stride of 20. The data is augmented by random flipping and rotation. For test, D3Dnet employs the Vid4 dataset. D3Dnet uses MSE as the loss function and Adam as the optimizer. The learning rate is initially set to 4×10^{-4} and halved for every 6 epochs.

5) *VESR-Net*: VESR-Net adopts the Youku-VESR dataset, which contains 1,000 video clips with 1080p. 50 videos are for test and the rest are for training. As for the training set, the LR frames are then randomly cropped to patches with size 64×64 . As for the test set, the frame size is unchanged. VESR-Net uses L1 loss as the loss function and Adam as the optimizer with $\beta_1 = 0.9$ and $\beta_2 = 0.999$. The learning rate is initially set to 1×10^{-4} and the weight decay parameter is 0.8 for every 20 epochs.

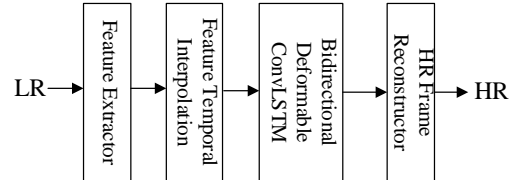


Fig. 38: The network architecture of STVSR [88].

6) *STVSR*: The architecture of space-time video super-resolution (STVSR)²⁶ [88] is shown in Fig. 38. STVSR can handle with both video super-resolution and video frame interpolation tasks. It is an end-to-end framework consisting of four parts: feature extractor, frame feature temporal interpolation module, bidirectional deformable ConvLSTM and HR frame reconstructor.

STVSR first uses a feature extractor with a convolutional layer and several residual blocks. The LR feature maps of intermediate frames are then synthesized with the proposed frame feature interpolation module. Furthermore, STVSR uses a bidirectional deformable ConvLSTM to process the consecutive feature maps and better leverage temporal information. It can simultaneously perform temporal alignment and aggregation by previous deformable convolutions before vanilla ConvLSTM [70]. Besides, it can process bidirectional motion of the

²⁶<https://github.com/Mukosame/Zooming-Slow-Mo-CVPR-2020>

features to collect more temporal information. Finally, the HR slow-motion video sequence is reconstructed from the aggregated feature maps by HR frame reconstructor with several residual blocks and a sub-pixel convolutional upscaling layer.

STVSR employs the Vimeo-90K dataset as training set, whose LR frames are then randomly cropped to patches with size 32×32 . And the data is augmented by random flipping and rotation. For test, STVSR adopts the Vid4 dataset and Vimeo as test set. To measure the performance of different methods under various motion conditions, the Vimeo test set is splitted into fast motion, medium motion and slow motion sets. All the metrics are calculated on Y channel. STVSR uses a reconstruction loss as the loss function and Adam as the optimizer. The learning rate is initially set to 4×10^{-4} and a cosine annealing is applied to reduce the rate to 10^{-7} .

XI. METHODS WITHOUT ALIGNMENT

A. 2D Convolution Methods

1) *VSRResFeatGAN*: The input frames of the generator are not aligned properly with multiple frames, but are up-sampled and fed directly into the network. It first conducts the 3×3 convolutional operation for each of multiple frames, and then the outputs are concatenated and conduct feature fusion via convolutional layers. The fused features are fed into multiple consecutive residual blocks, and finally the super-resolution result of the target frame is obtained by a 3×3 convolutional layer. The discriminator determines whether the output of the generator is a generated image or GT image. Then the result of the discriminator reacts to the generator, and promotes it to yield results closer to the GT images. Finally, a relative satisfactory solution is obtained through an iterative optimization.

In the training process, the generator is first trained, and then the generator and the discriminator are trained jointly. The loss function of VSRResNet consists of the adversarial loss, content loss, and perception loss, which is implemented by a VGG [100] to extract the features of the generated image and corresponding GT image, respectively, and then computing the loss using extracted features through the Cb loss function. The content loss denotes the Cb loss calculated between the generated result and GT.

Moreover, VSRResNet adopts the videos from *Myanmar*¹ as training set, Vid4 as testing set, and Adam as the optimizer. The number of input frames is set to 5 and the batch size is set to 64.

2) *FFCVSR*: The local network consists of 5 convolutional layers, 1 deconvolution layer, and 8 residual blocks, each of which is composed of 2 convolutional layers. The local network is responsible for producing corresponding features and HR target frame based on LR input frames. The context network consists of 5 convolutional layers, 1 deconvolution layer, 4 residual blocks, and 2 space-to-depth transformation layers.

FFCVSR consists of a local network and a context network, where the local network consists of 5 convolutional layers, 1 deconvolution layer, and 8 residual blocks, each of which is composed of 2 convolutional layers. The local network is responsible for producing corresponding features and HR target frame based on LR input frames. The context network consists of 5 convolutional layers, 1 deconvolution layer, 4 residual blocks, and 2 space-to-depth transformation layers.

Moreover, it has been found that simply inputting the previous recovered HR frames to the next context network leads to jitter and jagged artifacts. The solution is that for each sequence of T frames, the output of the current local network is used as the output of the previous context network. This method is called the suppression updating algorithm. The training set of FFCVSR comes from harmonicinc.com including Venice and Myanmar with resolution of 4K, and Vid4 is used as testing set. FFCVSR adopts MSE as the loss function, Adam as the optimizer. The initial learning rate is set to 10^{-4} .

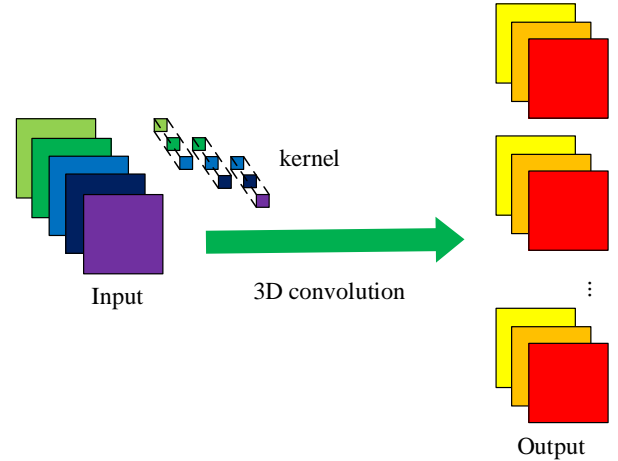


Fig. 39: The flowchart of 3D convolution.

B. 3D Convolution Methods

The flowchart of 3D convolution is shown in Fig. 39.

1) *DUF*: DUF also proposes a data augmentation method in the temporal axis for video data. By sampling frames in order or in reverse order at different time intervals, videos with different motion speed and directions can be obtained. In the experiment, DUF uses the Huber function as its loss function, where $\delta = 0.01$. Adam is used as the optimizer, and the initial learning rate is set to 10^{-3} .

2) *FSTRN*: In the experiment, FSTRN uses 25 video sequences with the YUV format as training set, videos in [101] as testing set (including Dancing, Flag, Fan, Treadmill and Turbine). The number of input frames is 5. The Cb function is used as the loss function, and Adam is used as the optimizer for training the network. The initial learning rate is set to 10^{-4} and the patch size is set to 144×144 .

3) *3DSRnet*: The SR result is obtained by adding the residual image that is learned by the network with the bicubic-interpolated LR target frame. As the network goes deeper, the depth of feature maps after 3D convolution becomes shallower as well. In order to keep the depth and retain temporal information, 3DSRNet adopts an extrapolation operation, which adds one frame at the beginning and the end of the consecutive frames, respectively.

In experimental settings, the kernel size of 3D convolutional is $3 \times 3 \times 3$. 3DSRNet uses MSE as its loss function, Adam as the optimizer, and Xavier as the method of weight initialization. The number of input frames is 5.

C. Recurrent Convolutional Neural Networks

1) *BRCN*: In the forward subnet, the input of each node in the hidden layer comes from three parts: the output of the previous layer at the current time t , and at time $t - 1$, and the output of the previous node in the current layer, respectively. Note that these three outputs are all resulted from the corresponding convolutional operation, which are named as feedforward convolution, conditional convolution and recurrent convolution, respectively. The feedforward convolution is used to extract spatial dependence, while the other two convolutions are used to extract temporal dependence among consecutive frames. Finally, the output of the whole network is the combination of the output from the two sub-networks as follows: the output of the feedforward convolution at the current time t and the output from the conditional convolution at time $t - 1$ in the forward sub-network, the output of the feedforward convolution at the current time t and the output from the conditional convolution at time $t + 1$ in the backward sub-network.

BRCN uses 25 video sequences in the YUV format as the training set, and the video sequences in [101] as testing set. The patch size is 32×32 , the number of input frames is 10, and MSE is as its loss function. The network is optimized through stochastic gradient descent (SGD) algorithm.

2) *STCN*: Firstly, multiple consecutive up-sampled LR video frames are taken as input and then each frame is convoluted in the spatial module to extract features. Then the outputs are sent to the BMC-LSTM recurrent layer in the temporal module to extract temporal correlation. BMC-LSTM is a bidirectional multi-scale convolution variant of LSTM. Finally, a convolution is performed to attain the HR result of the target frame. The spatial module is composed of 20 convolutional layers with kernel size 3×3 , where the number of kernels is 64. The temporal module consists of three layers, each of which consists of multiple BMC-LSTM submodules.

The number of input frames for STCN is 5. Under this condition, the corresponding spatial module consists of 5 branches and each branch has 20 convolutional layers. The temporal module consists of 3 layers and each has five BMC-LSTM submodules. Then the reconstruction

module consists of 1 convolutional layer. STCN adopts MSE as its loss function. In particular, the loss function calculates the difference between the reconstruction result of the adjacent frames and the corresponding HR frame, as well as the difference between the reconstruction result of the target frame and the corresponding HR frame. During training, the weight of the loss of the adjacent frame in its total loss is controlled by gradually decaying the balance parameter from 1 to 0. Besides, STCN uses Adam as the optimizer with batch size 64, and initial learning rate is 10^{-4} .

3) *RISTN*: In the experiment of [50], RISTN randomly selects 50K images from the ImageNet dataset to pre-train the spatial module and then uses 192 videos with resolution $1,920 \times 1,080$ collected from 699pic.com and vimeo.com as the training set to train the whole network. RISTN uses the mean MSE as its loss function, and the sparse matrix is constrained by the ℓ_1 -norm regularization term. Besides, the number of input frames is set to 5. The super-resolution scale is 4, and Vid4 is used as testing set.

D. Non-Local Methods

An example for f function is given below. It is a spatio-temporal non-local block, where f is an embedded Gaussian function as follows:

$$f(x_i, x_j) = e^{\theta(x_i)^T \phi(x_j)} \quad (15)$$

where $\theta(x_i) = W_\theta x_i$, $\phi(x_j) = W_\phi x_j$, and $\mathcal{C}(x) = \sum_j f(x_i, x_j)$.

The non-local block can easily be added into existing deep convolutional neural networks. Although non-local networks are able to capture spatio-temporal information effectively, the disadvantage, which is similar to 3D convolution, is that it has a large amount of computation.

1) *PFNL*: In addition, in order to avoid the increase of parameters brought by the superposition of PFRB, PFNL adopts the mechanism of parameter sharing between channels (refer to [102, 103]), which effectively balances trade-off between the number of parameters and network performance. PFNL chooses the Cb function as its loss function, and uses Adam as the optimizer and 10^{-3} as its initial learning rate.

2) *MuCAN*: MuCAN employs the Vimeo-90K and REDS (except REDS4) dataset as training sets, whose LR frames are then randomly cropped to patches with size 64×64 . The data is augmented by random flipping and rotation. For test, MuCAN adopts REDS4 and Vimeo-90K-T dataset without boundary cropping. The metrics are calculated only on RGB channel on REDS4, while they are on both RGB and Y channels on V-test. MuCAN uses an Edge-Aware loss as the loss function to dispose the effects of jagged edges and ensure the generation of refined edges. The optimizer of MuCAN is Adam with learning rate initially set to 4×10^{-4} and a cosine annealing is applied to reduce the rate.

XII. PERFORMANCE COMPARISONS

A. Performance of Methods

The performance of the representative video super-resolution methods with magnification factors 2 and 3 are given in Table V in terms of both PSNR and SSIM. The degradation types are the bicubic downsampling with the image-resize function (BI) and Gaussian blurring and downsampling (BD). Note that all the PSNR and SSIM are cited from the original works. And a simple comparison on the performance may not be fair, since the training data, the pre-processing, and the cropped area in videos are likely totally different in those methods.

In $\times 2$ and $\times 3$ VSR tasks, the top 3 methods on Vid4 test set which contains large amounts of high frequency details, under BI degradation are MMCNN, RRCN and 3DSRnet.

ACKNOWLEDGMENT

We thank all the reviewers for their valuable comments. This work was supported by the National Natural Science Foundation of China (Nos. 61976164, 61876220, 61876221, 61836009 and U1701267), the Project supported the Foundation for Innovative Research Groups of the National Natural Science Foundation of China (No. 61621005), the Program for Cheung Kong Scholars and Innovative Research Team in University (No. IRT_15R53), the Fund for Foreign Scholars in University Research and Teaching Programs (the 111 Project) (No. B07048), the Science Foundation of Xidian University (Nos. 10251180018 and 10251180019), the National Science Basic Research Plan in Shaanxi Province of China (Nos. 2019JQ-657 and 2020JM-194), and the Key Special Project of China High Resolution Earth Observation System-Young Scholar Innovation Fund.

TABLE V: Comparison of all the methods on the datasets with scale factors 2 and 3. Noted that 'Internet' means that the dataset is collected from the internet. '*' denotes that the source of the dataset is unknown, and '-' indicates that the method does not be tested on the datasets.

Method	TrainSet	TestSet	Scale	BI		BD	
				PSNR	SSIM	PSNR	SSIM
VSRnet [20]	Myanmar	Vid4	×2	31.30	0.9278	-	-
		Myanmar-T		38.48	0.9679	-	-
3DSRnet [46]	largeSet	Vid4		32.25	0.9410	-	-
		Vid4		33.50	0.9491	-	-
MMCNN [29]	*	Myanmar-T		39.37	0.9740	-	-
		YUV21		34.96	0.9371	-	-
DRVSR [22]	*	SPMCS		36.71	0.9600	-	-
VSRResNet [42]	Myanmar	Vid4		31.87	0.9426	-	-
		Vid4		-	-	28.77	0.8499
BRCN [48]	YUV25	TDTFF		-	-	32.84	0.8968
		Myanmar-T		40.47	0.9800	-	-
RRCN [32]	Myanmar	Vid4		33.41	0.9490	-	-
		YUV21		35.62	0.9425	-	-
DUF [44]	Internet	Vid4		-	-	33.73	0.9554
STCN [49]	*	Hollywood2		-	-	41.51	0.9804
VSRnet [20]	Myanmar	Vid4	×3	26.79	0.8098	-	-
		Myanmar-T		34.42	0.9247	-	-
VESPCN [21]	CDVL	Vid4		27.25	0.8447	-	-
3DSRnet [46]	largeSet	Vid4		27.70	0.8498	-	-
		Vid4		28.40	0.8722	-	-
MMCNN [29]	*	Myanmar-T		35.42	0.9393	-	-
		YUV21		30.82	0.8567	-	-
DRVSR [22]	*	Vid4		27.49	0.8400	-	-
		SPMCS		31.92	0.9000	-	-
VSRResNet [42]	Myanmar	Vid4		27.80	0.8571	-	-
		Myanmar-T		35.53	0.9446	-	-
RRCN [32]	Myanmar	Vid4		28.25	0.8618	-	-
		YUV21		31.35	0.8668	-	-
DUF [44]	Internet	Vid4		-	-	28.90	0.8898
STCN [49]	*	Hollywood2		-	-	37.03	0.9546